이학박사 학위논문

Cohesin을 매개로 하는 다이나믹한 크로마틴의 higher-order chromatin 구조가 tumor development에 미치는 영향 규명

Dynamic higher-order chromatin structure mediated by cohesin complex contributes to tumor development

2016 년 8 월

서울대학교 융합과학기술대학원

분자의학 및 바이오 제약 학과

윤 지 연

Cohesin을 매개로 하는 다이나믹한 크로마틴의 higher-order chromatin 구조가 tumor development에 미치는 영향 규명

지도교수 김 태 유

이 논문을 이학박사 학위논문으로 제출함.

2016년 8월

서울대학교 융합과학기술대학원

분자의학 및 바이오 제약 학과

윤 지 연

윤 지 연의 이학박사 학위논문을 인준함.

2016년 8월

위 원 장 강경호 (인)

부위원장 김 태 유 (인)

위 원 윤 홍 덕 (인)

위 원 예 상 규 (인)

위 원 [illegible] (인)

Dynamic higher-order chromatin structure mediated by cohesin complex contributes to tumor development

By

Jiyeon Yun

(Directed by Tae-You Kim, M.D., Ph.D.)

A thesis submitted in partial fulfillment of the requirements for the Degree of Doctor of Philosophy in Department of Molecular Medicine and Biopharmaceutical Sciences World Class University Graduate School of Convergence Science and Technology Seoul National University, Seoul, Korea

August, 2016

Approved by thesis committee:

Professor Gyeong Hoon Kang **Chairperson**

Professor Tae-You Kim **Vice Chairperson**

Professor Hongdae Yoon

Professor Sang-Kyu Ye

Professor Young-Joon Kim

ABSTRACT

Dynamic higher-order chromatin structure mediated by cohesin contributes to tumor development

Jiyeon Yun

Major in Cancer Epigenetics

Department of Molecular Medicine and Biopharmaceutical Sciences

Graduate School of Convergence Science and Technology

Seoul National University

Higher-order chromatin architecture is known to be important to gene regulation during hematopoiesis, erythropoiesis, and development. Chromatin architectural molecule cohesin complex tightly and dynamically controls genomic organization to regulate transcript splicing, gene transcription, and chromosomal instability in cancer. Although substantial evidences have shown that cohesin

complex is involved in tumorigenesis, the effects of chromatin architecture-mediated by cohesin complex on tumor development are still unclear.

Here, we show that 1) highly amplified genes form typical long-range chromatin interactions, which are stabilized by enriched cohesin. Impaired cohesin complex inhibits DNA replication initiation by reducing the recruitment of pre-replication complexes such as minichromosome maintenance subunits 7 (MCM7), DNA polymerase α, and CDC45 at replication origins near the amplified regions, and as a result, decreases the DNA copy numbers of highly amplified genes. Collectively, our data demonstrate that cohesin-mediated chromatin organization and DNA replication are important for stabilizing gene amplification in cancer cells with chromosomal instability.

Next, 2) we report that cohesin-mediated chromatin organization initiates and coordinates EMT by activating mesenchymal genes. Depletion of RAD21 in epithelial cancer cells causes transcriptional activation of TGFB1 and ITGA5, inducing EMT. Reduced binding of RAD21 changes intrachromosomal chromatin interactions within the TGFB1 and ITGA5 loci, creating an active transcriptional environment. Similarly, stem cell-like cancer cells also show an open chromatin structure at both genes, which correlates with high expression levels and mesenchymal fate characteristics. These findings indicate that dynamic cohesin-mediated chromatin structures are responsible for the initiation and regulation of essential EMT-related cell fate changes in cancer.

Key words: Cohesin, higher-order chromatin structure, gene amplification, epithelial-mesenchymal transition, cancer stem cell, cancer metastasis

Student Number : 2009-24114

TABLE OF CONTENTS

ABSTRACT ---------- **i**

TABLE OF CONTENTS ---------- **iv**

LIST OF TABLES AND FIGURES ---------- **vi**

Ⅰ. REDUCED COHESIN DESTABILIZES HIGH-LEVEL GENE AMPLIFICATION BY DISRUPTING PRE-REPLICATION COMPLEX BINDINGS IN HUMAN CANCERS WITH CHROMOSOMAL INSTABILITY ---------- 1

ABSTRACT ---------- 2

INTRODUCTION ---------- 3

MATERIALS AND METHODS ---------- 6

RESULTS ---------- 13

DISCUSSION ---------- 36

Ⅱ. DISRUPTION OF INTRACHROMOSOMAL INTERACTIONS BY DEFICIENT COHESIN INITIATE EPITHELIAL-MESENCHYMAL TRANSITION AND STEMNESS IN CANCER ---------- 40

ABSTRACT ---------- 41

INTRODUCTION ---------- 42

MATERIALS AND METHODS ---------- 45

RESULTS ---------- 50

DISCUSSION ---------- 77

REFERENCES ---------- 82

ABSTRACT IN KOREAN ---------- 90

ACKNOWLEDGEMENT ---------- 93

LIST OF TABLES AND FIGURES

Ⅰ. REDUCED COHESIN DESTABILIZES HIGH-LEVEL GENE AMPLIFICATION BY DISRUPTING PRE-REPLICATION COMPLEX BINDINGS IN HUMAN CANCERS WITH CHROMOSOMAL INSTABILITY

TABLE 1. Chromosomal segment with simultaneously altered DNA copy-number and expression following RAD21-KD. ---------- 17

Figure 1. Stable down-regulation of cohesin does not led to mitotic arrest or the development of chromosomal segregation defect in SNU16 cells. ---------- 14

Figure 2. Reduction of cohesin leads to transcriptional inefficiency of the APIP/PDHX/CD44 locus in SNU16 cells ---------- 20

Figure 3. Copy-numbers of amplified APIP/PDHX/CD44 locus are decreased by cohesin reduction in SNU16 cells. ---------- 24

Figure 4. Down-regulation of cohesin impairs localization of pre-replication complex at replication origins within the amplified APIP/PDHX/CD44 locus. -- 28

Figure 5. Copy-numbers of amplified gene existing in HSRs are decreased by cohesin reduction. ---------- 31

Figure 6. Copy-numbers of amplified gene existing in DMs are decreased by cohesin reduction. ---------- 33

Figure 7. Proposed model for cohesin-mediated copy-number loss of highly amplified genes existing on DMs and HSRs in human cancer cells. ---------- 35

Ⅱ. DISRUPTION OF INTRACHROMOSOMAL INTERACTIONS BY DEFICIENT COHESIN INITIATE EPITHELIAL-MESENCHYMAL TRANSITION AND STEMNESS IN CANCER

Figure 1. Unstable RAD21 mRNA leads to low level of RAD21 protein in Mesenchymal breast cancer cells. ---------- 52

Figure 2. Reduction of RAD21 induces TGFB1 and ITGA5 transcription. -------56

Figure 3. Disrupted RAD21 causes morphological changes from epithelial-like into fibroblast-like shapes. ---------- 61

Figure 4. Released chromatin loop structure in TGFB1 and ITGA5 genes by RAD21KD leads to the recruitment of active transcription factors to the gene promoter. ---------- 65

Figure 5. RAD21 is responsible for metastatic characteristics in CSLCs. -------- 71

Figure 6. RAD21 overexpression in MDA-MB-231 mesenchymal cancer cells decreases TGFB1 and ITGA5 expression with enhanced intra-chromosomal interactions. ----------74

Ⅰ. Reduced cohesin destabilizes high-level gene amplification by disrupting pre-replication complex bindings in human cancers with chromosomal instability

ABSTRACT

Gene amplification is a hallmark of cancer with chromosomal instability although the underlying mechanism by which altered copy numbers are maintained is largely unclear. Cohesin, involved in sister chromatid cohesion, DNA repair, cell cycle progression, and transcriptional regulation of key developmental genes, is frequently over-expressed in human cancer. Here we show that cohesin-dependent change in DNA replication controls the copy numbers of amplified genes in cancer cells with chromosomal instability. We found that the down-regulation of elevated cohesin leads to copy number-associated gene expression changes without disturbing chromosomal segregation. Highly amplified genes form typical long-range chromatin interactions, which are stabilized by enriched cohesin. The spatial proximities among cohesin binding sites within amplified genes are decreased by *RAD21*-knockdown, resulting in the rapid decline of amplified gene expression. After several passages, cohesin depletion inhibits DNA replication initiation by reducing the recruitment of pre-replication complexes such as minichromosome maintenance subunits 7 (MCM7), DNA polymerase α, and CDC45 at replication origins near the amplified regions, and as a result, decreases the DNA copy numbers of highly amplified genes. Collectively, our data demonstrate that cohesin-mediated chromatin organization and DNA replication are important for stabilizing gene amplification in cancer cells with chromosomal instability.

Key words : Cohesin, higher-order chromatin structure, gene amplification, cancer

INTRODUCTION

In order to maintain genome integrity, genetic and epigenetic alteration is strictly regulated during mammalian development [1]. However, genomic instability, including deletion/insertion, alternations in chromosome number, chromosome translocations, and gene amplifications, is frequently observed in human cancer [2]. The continuous accumulation of genomic instability leads to an imbalance in aneuploidy, an increased rate of loss-of-heterozygosity, and gains or losses of whole or partial chromosomes that is called chromosomal instability (CIN) [2, 3].

Gene amplification, which is observed in many types of cancer with CIN [4], drives tumor progression by increasing the expression of oncogenes such as *c-Myc*, *HER2*, and *EGFR* [5]. The extra copies of amplified DNA in human cancers can be organized as cytologically visible homogeneously staining regions (HSRs) and extrachromosomal double minutes (DMs) [4]. DMs, an autonomously replicating extrachromosomal circular DNA, can be initiated by somatic genome rearrangement through DNA breakage and repair processes (called the breakage-fusion-bridge (BFB) cycle) in human cancers [6, 7]. The creation of DNA double strand breaks (DSBs) followed by replication stress and fusion of chromosome ends results in an unstable dicentric chromosome, which leads to the accumulation of additional DNA breaks [7, 8]. Thus, continuous DSBs formation and subsequent inaccurate DNA repair may provoke the amplification of DMs near the breakage sites [4, 9]. DMs are delivered to the daughter cell by attaching to the mitotic

chromosome during mitosis [7]. In addition, DMs can be integrated into the chromosome arm, followed by repeated initiation of BFB cycle triggered by site-specific DSBs, finally leading to HSRs formation [7, 10]. However, the molecular mechanisms responsible for maintaining gene amplification in human cancers are not completely understood yet. Since gene amplification not only confers a selective advantage during tumor development but also minimizes sensitivity to anti-cancer drugs [11], therefore, understanding the maintenance processes operating for amplified genes may provide an opportunity to overcome drug resistance caused by oncogene amplification [9, 11].

Cohesin is composed of four major core subunits: SMC1, SMC3, RAD21, and SCC3 [12]. This complex was originally found to be involved in sister chromatid cohesion, DNA repair, and cell cycle progression [13, 14]. Thus, mutational inactivation of the cohesin complex causes CIN and aneuploidy in human cancer cells due to improper chromosome segregation fidelity [15, 16]. In addition to its major influence on sister-chromatid cohesion and DNA repair, the cohesin complex affects gene transcription by facilitating long-range interactions among members of many developmentally regulated gene families [17-22]. Interestingly, aberrant expression of cohesin components is also present in many human cancers [23]. The recent discovery that the over-expression of cohesin components confers poor prognosis and resistance to chemotherapy in breast and colorectal cancers [24, 25] rasises the possibility that the elevated cohesin level is essential for tumorigenesis [23]. However, it is not yet clear if enhanced expression of cohesin can contribute to

the gene amplification process.

In the present investigation, we comprehensively evaluated the effects of cohesin reduction on gene amplification. We found that the down-regulation of elevated cohesin abolishes long-range chromatin interactions of highly amplified genes with a concurrent reduction of transcription in human gastric cancer cells. Moreover, reduction of cohesin appears to de-stabilize high-level gene amplifications by disrupting the recruitment of pre-replication complex to the near amplified genes in chromosomally unstable cancer cells, thereby reducing DNA copy-number of amplified genes.

MATERIALS AND METHODS

1. Patient tissues, cell culture, virus production, transduction, and cell-growth inhibition assay

Twenty four human gastric tumor tissues and the matched normal tissues were obtained from the Tissue Bank of Seoul National University Hospital. The study protocol was reviewed and approved by the institutional review board of Seoul National University Hospital. Four CIN^+ cell types (SNU16, N87, COLO 320-HSR, and COLO 320-DM) with multiple chromosomal structure changes and three CIN^- cancer-cell types (HCT116, LoVo, and HepG2 cells; diploid/near-diploid karyotype with a few structural alterations) were obtained from American Tissue Culture Collection or the Korean Cell Line Bank and have not been cultured for longer than 6 months. Cells were cultured in DMEM or RPMI 1640 supplemented with 10% fetal bovine serum and gentamicin (10 μg/mL) at 37 °C in a 5% CO^2-humidified atmosphere [7, 15, 26-29]. Control and RAD21-directed TRC lentiviral shRNAs were purchased from Open Biosystems. Lentiviruses were produced by transducing 293FT cells with shRNA using a Virapower packaging mix (Invitrogen) as previously described [30]. The viruses were harvested from the media on day 3 by centrifugation, and cells were then incubated with viral supernatant in the presence of 6 μg/mL polybrene (Sigma). After 2 days of incubation, the transduced cells were cultured in the presence of 1 μg/mL puromycin (Sigma) for another 3 days before collection as previously described [17]. Silencing was confirmed by western

blot analysis and qPCR. To generate stably transfected cells, several single colonies were isolated and independently expanded in the presence of puromycin as previously described [30]. Flow cytometry was performed as previously described [17]. Cell-growth inhibition was measured by an MTT assay as previously described [31].

2. Reverse transcription and western blot analysis

Two μg total RNA was reverse transcribed with random hexamers as previously described [22, 32]. Whole cell extracts were prepared, and western blot analysis was performed as previously described [31].

3. Array-comparative genome hybridization (array-CGH) analysis

Genomic DNA from cells was analyzed by array-CGH [33] using a 2 × 400K oligonucleotide microarray (Agilent Technologies) according to the manufacturer's recommendations as previously described [34]. Test DNA (2 μg) and reference DNA (2 μg) was digested with AluI and RsaI (Promega). The digested test DNA and reference DNA were labeled with cyanine (Cy) 3-deoxyuridine triphosphate (dUTP) or Cy5-dUTP, respectively, using an Agilent Genomic DNA Labeling Kit PLUS (Agilent). The individually labeled test and reference samples were then purified using Microcon YM-30 filters (Millipore, Billerica, MA).

Following purification, the Cy3-labeled test DNA and Cy5-labeled reference DNA were mixed together and combined with 2× hybridization buffer (Agilent), 10× blocking agent (Agilent), and human *Cot-1* DNA (Invitrogen). The hybridization mixture was slowly dispensed onto a microarray chip and assembled with an Agilent SureHyb chamber (Agilent). The assembled slide chamber (Agilent) was placed in the rotator rack in a hybridization oven for 40 h at 65°C with suitable rotation. Hybridization was followed by two washes with Washing Buffer 1 and Washing Buffer 2 (Agilent) according to the manufacturer's instructions. After washing, all microarray slides were scanned with an Agilent Microarray Scanner G2505C at a 5-μm resolution. Captured images were transformed into data with Feature Extraction Software, version 10.7 (Agilent), and then imported into Agilent CGH Analytics 5.0.14 software for evaluation. From the array-CGH data, we subtracted the background intensity from the total spot intensity. To remove systematic bias of the chip, within-slide normalization was performed using Lowess normalization for log2 transformed data. Copy number data for the target and control samples were manually inspected. Probe-level data was segmented using the circular binary segmentation method [35] to detect statistically significant CNA values. Copy number gain or loss beyond log2 (RAD21-shRNA/control-shRNA) ± 0.3 was catalogued for each sample. All calculations were performed using R.

4. Paired-end transcriptome analysis

Sequencing libraries were generated according to the standard protocol of

Illumina Inc. for high-throughput sequencing. The transcriptome was then sequenced using a Genome Analyzer IIx (Illumina Inc.) as previously described [34]. We mapped 101-bp sequenced fragments to the human genome using TopHat2.0.8, which can allow up to two mismatches with the references. Sequenced reads were aligned to human transcript reference sequences from the UCSC database (Homo_sapiens.GRCh37/hg19) for expression analysis at the gene/transcript levels [36]. We use the DEGseq R package program to detect differential expression mainly because this software supports an experimental design between two samples without multiple technical replicates [37]. We identified differentially expressed genes (DEGs) according to the overall differential expression from the DEGseq analysis with $FDR < 0.001$.

5. CNV assay

Cells and human primary gastric cancer tissues and matched normal samples were assayed for gene copy number using TaqMan Gene Copy Number Assays [38]. Each probe was designed based on a genomic sequence (Homo_sapiens.GRCh37/hg19) using Applied Biosystems proprietary software. Each assay was run as a TaqMan real-time PCR reaction in triplicate, using an FAM dye–based assay targeted to 11p13 and a VIC dye–based assay for the reference gene, RNase P (PN 4316844 from Applied Biosystems). Each 20 μL PCR reaction contained 20 ng gDNA and TaqMan probe/primer mix in TaqMan Universal Master Mix, and was amplified using StepOnePlus (Applied Biosystems). Cycling

conditions were 2min at 50°C and 10 min at 95°C, followed by 40 cycles of 15 sec at 92°C and 60 sec at 60°C. Real-time data were collected by CopyCaller v2.0 software. This method involved the relative quantification of the test sequence versus a reference gene known to have two copies per diploid genome. Relative quantity was determined using the ΔΔCt [(FAM Ct – VIC Ct) sample – (FAM Ct – VIC Ct) calibrator] method [17] in which a reference sample or calibrator known to have two copies of the test sequence is used as the basis for comparison.

6. Fluorescent *in situ* hybridization (FISH)

Cells were fixed with Carnoy's solution on slides and then dried. The cells were then covered with 10 μL dual hybridization mixture containing a pair of painting probes and labeled with two different fluorochromes. The painting probes were labeled with MacProbe™ solution (Macrogen). The slides and probes were denatured at 75°C for 2 min and hybridized overnight at 37°C. Post-hybridization washes were conducted according to the manufacturer's protocol.

7. Chromatin immunoprecipitation (ChIP) assay and quantitative real-time PCR (qPCR)

ChIP assays were performed as previously described [22, 30]. qPCR using SYBR Green (Molecular Probes) was performed to observe enriched DNA or cDNA

using StepOnePlus (Applied Biosystems) as previously described [32]. The enrichment of target DNA over the input was calculated using the ΔΔCt method, and the results were presented as the mean ± SEM [17, 30, 39]. The PCR primers used for the ChIP and qPCR assays are available upon request.

8. Chromosome conformation capture (3C) assay

A 3C assay was performed as previously described [22, 40, 41] with minor modification. Briefly, chromatin crosslinked in 1% formaldehyde was digested with 1000 U of EcoRI (NEB) overnight followed by ligation with 2000 U of T4 DNA ligase (NEB) at 16°C for 4h. Crosslinking was reversed, and the DNA was then purified by phenol extraction and ethanol precipitation as previously described [30]. To generate control templates for the positive controls, equimolar amounts of the different BAC clones were mixed and digested with 200 U of EcoRI overnight at 37°C as previously described [42]. After phenol extraction and ethanol precipitation, DNA fragments (200 ng/μL) were ligated with T4 DNA ligase. Digestion efficiency was calculated as previously described [43] and samples with efficiencies greater than 90 % were used for the 3C assays. Crosslinking frequency and ligation efficiencies between different samples were normalized relative to the ligation frequency of two adjacent EcoRI fragments in the *CalR* gene [41]. Quantitation of the data was performed by qPCR using SYBR Green (Molecular Probe).

9. Antibodies

Antibodies specific for the following factors were used in this study: c-Myc (SC-40), normal rabbit IgG (SC-2027), CDC45 (SC-20685), and RNA pol II (SC-899) from Santa Cruz Biotechnology; RAD21 (ab992) and DNA Pol α (ab31777) from AbCam, and CTCF (07-729) from Millipore. Anti-CD44 antibody (5640S) and anti-MCM7 (3735S) was purchased from Cell Signaling Technology. Anti-SMC1 antibody (A300-055A) was from Bethyl Lab.

10. Immunofluorecsence analysis

Cells were seeded on 0.01% poly-L-lysine (Sigma-Aldrich)–coated coverslips. Next day, the coverslips were rinsed once in PBS (37°C), fixed in 4% formaldehyde for 15 minutes, permeabilized with 0.5% Triton X-100 for 5 minutes, and then

RESULTS

1. Reduction of cohesin induces neither mitotic arrest nor defective chromosomal segregation in SNU16 cells

First, to explore if elevated cohesin level is required to maintain gene amplification, we stably reduced the expression of cohesin by RAD21-knockdown (KD) in SNU16 human gastric cancer cells with multiple chromosomal instability (CIN^+) [27, 29]. RAD21 is a core subunits of the cohesin complex [12]. Two different RAD21-directed shRNAs reduced RAD21 expression with a similar efficiency, thus decreasing RAD21 mRNA and protein levels by approximately 90% in SNU16 cells (Figure 1A and B). In contrast, the levels of CTCF, which position cohesin on its site [44], were not affected in RAD21-KD SNU16 cells (Figure 1A and B). Using FACS analysis we observed that stable RAD21-KD SNU16 cells seemed to exit mitosis, and then divided and survived well without pronounced cell death (Figure 1C). Moreover, following treatment with nocodazol, a microtubule polymerization inhibitor [16], we also found that stable RAD21-KD does not induce aberrant sister chromatid separation (Figure 1D and E). Collectively, we conclude that the stable down-regulation of cohesin by RAD21-KD induces neither mitotic arrest nor defective chromosomal segregation during mitosis and meiosis in SNU16 cells with CIN^+. We obtained similar results in three CIN^+ (N87, COLO 320-HSR, and COLO 320-DM) [7] and three cancer cells with stable chromosomes (CIN^-) (HCT116, LoVo, and HepG2) [15, 16, 26].

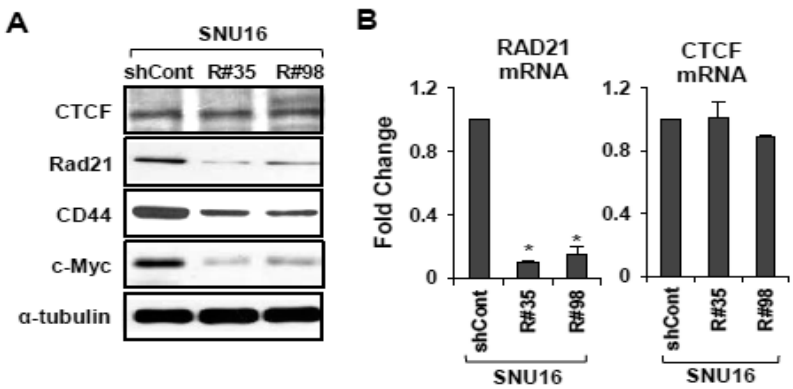

Figure 1. Stable down-regulation of cohesin does not led to mitotic arrest or the development of chromosomal segregation defect in SNU16 cells (**A, B**) SNU16 cells were stably transduced with control GFP-shRNA or two different RAD21-shRNAs (R#35 and R#98). (**A**) Western blot analysis was performed with the indicated antibodies on day 60 after RAD21-KD in SNU16 cells. α-tubulin served as a loading control. (**B**) RAD21 or CTCF mRNA expression was analyzed by qRT-PCR on day 60 after RAD21-KD in SNU16 cells. Each value was normalized to that of 18S ribosomal RNA relative to the control GFP-shRNA expressing SNU16 cells. Error bars represent the SD, n=3 biological replicates from independent viral transduction. *$P < 0.01$; Student's *t* test.

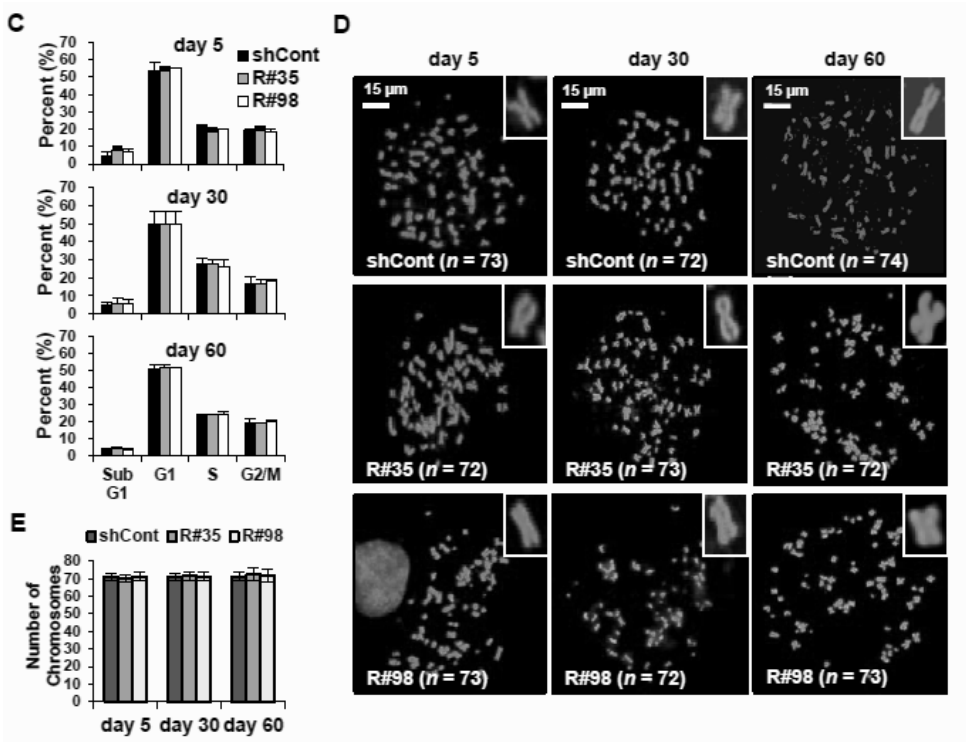

Figure 1. (**C**) SNU16 cells were stained with propidium iodide at the day 5, 30, and 60 after RAD21-KD, and then subjected to FACS analysis. The percentage of cells in the Sub G1, G1, S, and G2/M phases are shown. (Mean ± SD, n = 3 biological replicates). (**D**) A metaphase chromosome spread was prepared by treatment with nocodazol, a microtubule polymerization inhibitor [16], at the day 5, 30, and 60 after RAD21-KD in SNU16 cells and then cells were stained with DAPI. Scale bar = 15 μm. (**E**) The total chromosome numbers of the control GFP-KD or RAD21-KD SNU16 cells populations were counted at the day 5, 30, and 60 after three independent viral transduction procedures. Fifty mitotic spreads were evaluated for each sample (± SD). Representative FISH images are shown in (**D**).

2. Reduction of cohesin coordinately leads to copy number-associated gene expression changes in SNU16 cells

To directly assess the influence of cohesin depletion on gene amplification, we systematically identified copy-number changes in RAD21-KD SNU16 cells. Using array-CGH analysis [34], we found that genome-wide copy-number alterations were observed in RAD21-KD SNU16 cells compared to the control GFP-shRNA expressing SNU16 cells. To further determine whether DNA copy-number alterations produce corresponding changes in gene expression, copy number-associated gene expression alterations were monitored in RAD21-KD SNU16 cells. First, to assess the transcriptional impact of cohesin reduction, we carried out paired-end transcriptome analysis [34] from the control GFP-KD or RAD21-KD SNU16 cells and identified global gene expression changes in RAD21-KD SNU16 cells. Next, genome-wide array-CGH data and transcriptional profiles were integrated to search for candidate target genes with concomitantly altered DNA copy numbers and gene expression levels following cohesin reduction (data not shown). By matching differentially expressed genes to the corresponding copy-number, we identified six segment regions, including the *WDR11* and *APIP/PDHX/CD44* locus (see below), in which altered expression significantly correlated with changes in DNA copy-number (Table 1). Taken together, our results suggest that reduction of cohesin by RAD21-KD coordinately lead to copy number-associated gene expression alterations in SNU16 cells.

Locus	Total Gene Count within locus	Significant genes
chr11:34860427-35313292	5	*APIP, CD44, PDHX*
chr10:122570938-122768158	3	*WDR11, WDR11-AS1*
chr2:222972322-224020814	5	*ACSL3, FARSB, SGPP2*
chr11:67330919-67584926	6	*ALDH3B1, NDUFS8, TCIRG1, UNC93B1*
chr17:38402788-38596962	7	*BRCA1, IFI35, NBR2, RPL27, VAT1*
chr20:25199983-25401162	4	*ABHD12, GINS1*

Table 1. Chromosomal segment with simultaneously altered DNA copy-number and expression following RAD21-KD

3. Cohesin-mediated long-range chromatin interactions is required for transcriptional efficiency of the *APIP/PDHX/CD44* locus in SNU16 cells

In order to investigate whether cohesin can directly regulate the expression of amplified genes, we evaluated the highly amplified *APIP/PDHX/CD44* locus in SNU16 cells. *APIP/PDHX/CD44* locus, whose expression was responsive to RAD21-KD, are localized within 500 kb in chromosome 11 (Figure 2A and B). Since CTCF plays important role in cohesin positioning on chromatin [44], we determined whether CTCF is present at the *APIP/PDHX/CD44* locus. A UCSC Genome Bioinformatics database (http://genome.ucsc.edu/) search for CTCF binding motifs across the *APIP/PDHX/CD44* locus revealed numerous putative candidate sites (Figure 2A). Chromatin immunoprecipitation (ChIP) assays showed that CTCF binds within the *APIP/PDHX/CD44* locus in SNU16 cells (Figure 2C). Each value was normalized with gene copy number to determine the correct signal per region (data not shown). Prominent bindings of RAD21 and SMC1, two members of the cohesin complex [12], were co-localized with CTCF in SNU16 cells (Figure 2D and E), suggesting that *APIP/PDHX/CD44* locus is a natural target of the CTCF and cohesin complex. Increasing evidence has recently indicated that cohesin, along with CTCF, mediates high-order chromatin structures among CTCF/cohesin binding sites for the transcriptional regulation of many developmentally regulated gene families [17-20, 22]. To test whether the *APIP/PDHX/CD44* locus forms typical long-range chromatin interactions through cohesin binding, we carried out a chromosome conformation capture (3C) analysis [40] to assess the proximity of chromatin across the *APIP/PDHX/CD44* locus. Because high levels of cohesin occupancy is apparent

in the CTCF/cohesin binding site at the 3' end of *CD44* in SNU16 cells (amplicon 11 in Figure 2D), the EcoRI restriction fragment containing this region was used as an anchor primer. The 3' end of *CD44* was found to strongly interact with the CTCF/cohesin binding sites within the coding region of *APIP*, the 3' end of *PDHX*, and the promoter region of *CD44* in SNU16 cells (blue line, Figure 2F). When we used primers complementary to the 3' end of *PDHX* as anchors (amplicon 7 in Figure 2D), we also found strong interactions between *PDHX* and both *APIP* and *CD44* in SNU16 cells (blue line, Figure 2G), suggesting that the *APIP/PDHX/CD44* locus has a high-order chromosome architecture in SNU16 cells. Next, we examined whether cohesin was crucial for the observed long-range chromatin interactions and gene expression. First, we confirmed that high level of *APIP* and *CD44* expression was reduced by RAD21-KD in SNU16 cells (Figure 2B). Second, our ChIP experiments showed that RAD21 and SMC1 enrichments at the *APIP/PDHX/CD44* locus in RAD21-KD SNU16 cells were reduced twofold on average compared with those in the control GFP-shRNA expressing cells (Figure 2D and E). Consistent with the decreased enrichment of cohesin, the physical proximity in the RAD21-KD SNU16 cells (red line, Figure 2F and G) was significantly lower (twofold) than that in the control GFP-KD cells (blue line, Figure 2F and G). We observed the down-regulation of cohesin enrichment and a reduction of long-range chromatin interactions between the CTCF/cohesin binding sites within these amplified regions as early as 5 days after RAD21-KD in SNU16 cells. Thereafter, gene expression of highly amplified *APIP/PDHX/CD44* was significantly reduced in RAD21-KD SNU16 cells. Collectively, these results suggest that cohesin-mediated high-order chromosome

architecture is required for transcriptional efficiency of the *APIP/PDHX/CD44* locus in SNU16 cells.

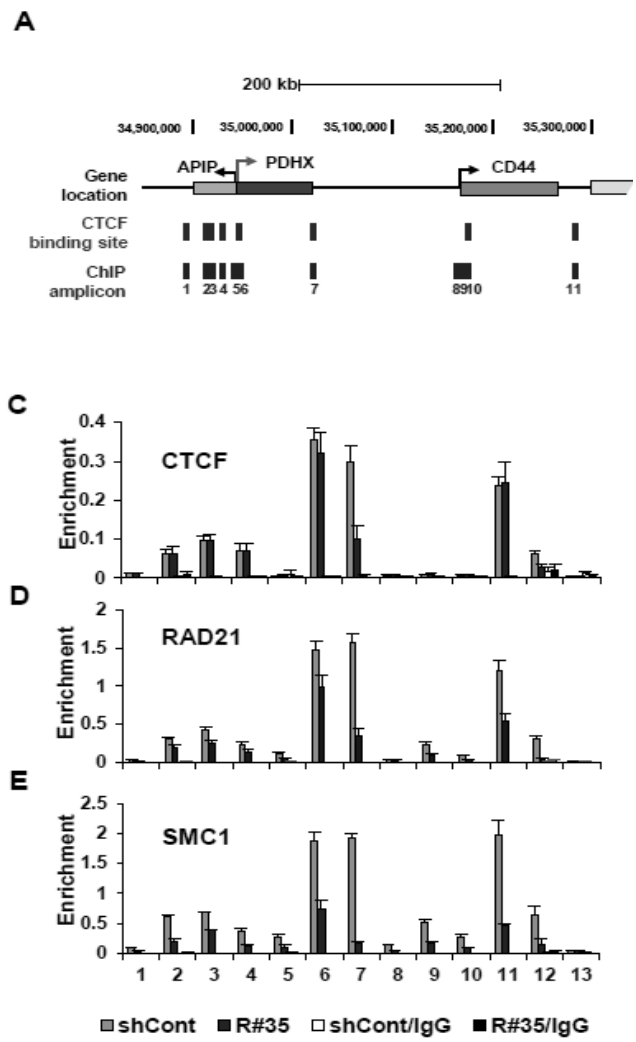

Figure 2. Reduction of cohesin leads to transcriptional inefficiency of the *APIP/PDHX/CD44* locus in SNU16 cells

(**A**) The *APIP/PDHX/CD44* locus at chromosome 11p13 is illustrated to scale. The

location of putative CTCF/cohesin binding sites and the primer pairs used for qPCR are shown with names below. (**C-E**) A ChIP assay was carried out with the control GFP-KD (blue bar) or RAD21-KD SNU16 cells (R#35; red bar) on day 60 after lentivial transduction using antibodies against to (**C**) CTCF, (**D**) RAD21, and (**E**) SMC1. The enrichment of target DNA over the input was calculated using the ΔΔCt method [17]. 3'HS1 (amplicon 12) of the human *β-globin* locus and *Necdin* (amplicon 13) served as positive and negative controls, respectively, for CTCF/RAD21 binding [17]. (Mean ± SEM, n = 3 biological replicates).

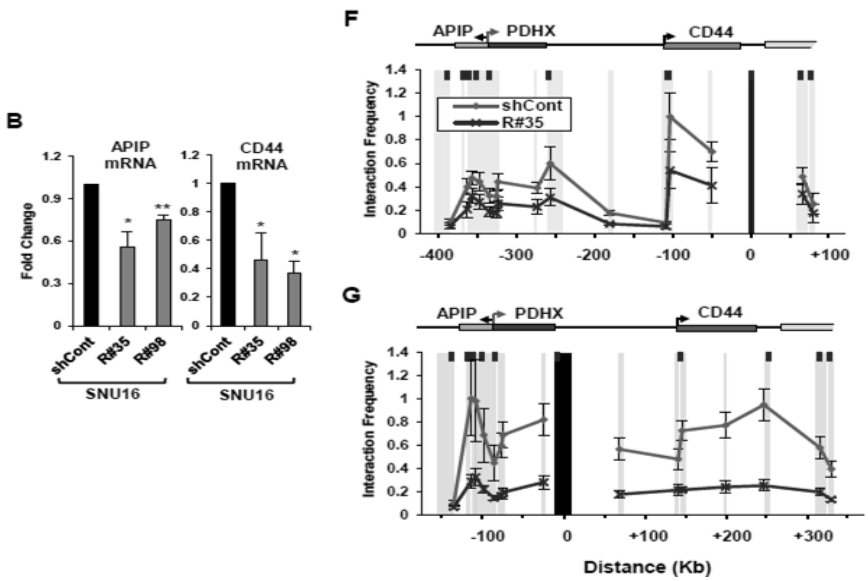

Figure 2. (**B**) APIP and CD44 expression was measured by qRT-PCR on day 60 after RAD21-KD in SNU16 cells. Each value was normalized to that of 18S ribosomal RNA relative to the control GFP-KD cells. (Mean ± SD, n = 3 biological replicates. (**F, G**) Relative crosslinking frequencies among CTCF/RAD21 binding sites within

the *APIP/PDHX/CD44* locus were measured with a 3C assay in the control GFP-KD (blue line) or RAD21-KD SNU16 cells (red line) on day 60 after lentivial transduction. The EcoRI restriction fragments in the *APIP/PDHX/CD44* locus appear as gray shaded bars. Black shading indicates the anchor fragment of (**F**) the 3' end of *CD44* and (**G**) the 3' end of *PDHX*. Each value was normalized to the crosslinking frequency at the *CalR* gene and the total DNA copy numbers to determine the correct signal per region [41]. The maximum crosslinking frequency was set to 1. (Mean ± SEM, n = 3 biological replicates).

4. Copy-numbers of amplified *APIP/PDHX/CD44* locus are decreased by cohesin reduction in SNU16 cells

Not only the gene transcription but also the amplified copy-number of the *APIP/PDHX/CD44* locus in SNU16 cells was notably reduced by RAD21-KD (Figure 3A). Interestingly, the amplified *APIP/PDHX/CD44* locus appeared as DMs (indicated as ① in Figure 3B), HSRs (indicated as ② in Figure 3B), and distributed insertions (indicated as ③ in Figure 3B) in parental SNU16 cells [4, 7]. Thus, to elucidate the copy-number changes induced by cohesin reduction with greater accuracy, a TaqMan-quantitative PCR-based CNV assay [38] targeting *APIP/PDHX/CD44* locus was performed. Compared with the two copies of *APIP* and *CD44* in the HCT116 cells, more than 100 copies of *APIP* and *CD44* were found in SNU16 cells (Figure 3C). Notably, the copy-number of *APIP* and *CD44* in the RAD21-KD SNU16 cells was significantly reduced relative to that in the control GFP-KD cells (Figure 3C). Next, FISH analysis of a metaphase spread of RAD21-KD SNU16 cells revealed that the amplified *APIP/PDHX/CD44* locus located in the HSRs was slightly reduced by RAD21-KD (Figure 3D). In addition, RAD21-KD in SNU16 cells also led to a decrease in the total number of DMs bearing the *APIP/PDHX/CD44* locus (Figure 3E), suggesting that cohesin reduction via RAD21-KD decreases the focal copy-number of amplified *APIP/PDHX/CD44* segments, which exist in both HSRs and DMs in SNU16 cells. DNA copy-numbers of *APIP* and *CD44* started to dwindle 30 days after viral transduction of RAD21-directed shRNAs and subsequently remained low throughout the rest of the experiment.

However, the copy-number changes of the same set of genes were not detected following RAD21-KD in HCT116, LoVo, and HepG2 cancer cells. Collectively, these results suggest that down-regulation of cohesin induces copy-number loss of amplified *APIP/PDHX/CD44* locus on HSRs and DMs only in CIN$^+$ SNU16 cells but not in other cancer cells having stable chromosome.

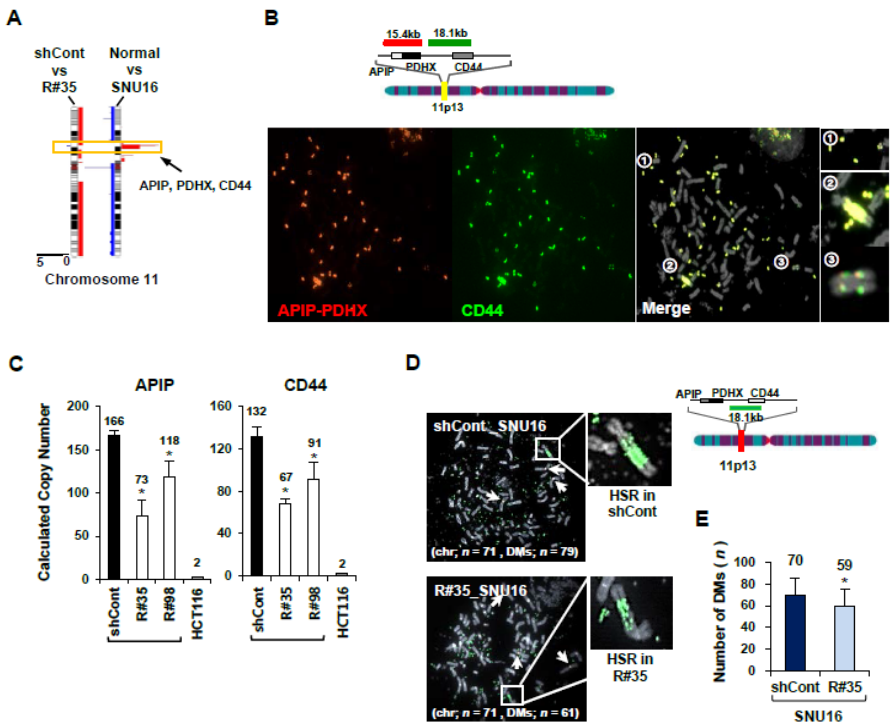

Figure 3. Copy-numbers of amplified *APIP/PDHX/CD44* locus are decreased by cohesin reduction in SNU16 cells.

(**A**) High-resolution array-CGH analysis was performed with the control GFP-KD or RAD21-KD SNU16 cells on day 60 after RAD21-KD. Chromosome 11 is represented by ideograms showing G-banding patterns (left ideogram, RAD21-KD

SNU16 cells compared with the control GFP-KD cells; right ideogram, parental SNU16 cells compared with normal gastric cells). Gains/amplifications (red) are shown on the right side of each ideogram, while losses (blue) appear on the left side. *APIP/PDHX/CD44* locus for further analyses are indicated by yellow boxes. (**B**) Localization of the FISH probes specific for *APIP/PDHX* (labeled with Cy3, red), and *CD44* (labeled with FITC, green) located on chromosome 11p13 is depicted. Metaphase FISH analysis of the *APIP/PDHX/CD44* locus on chromosome 11p13 in SNU16 cells revealed that two different probes co-localized on the same locus and exist in three types of amplification: DMs (①), HSRs (②), and distributed insertions (③). (**C**) Cohesin-mediated focal copy-number changes of *APIP* and *CD44* were evaluated using a TaqMan-quantitative PCR-based CNV assay with control GFP-KD or RAD21-KD SNU16 cells on day 60 after viral transduction. Data are presented as averages ± SD of biological triplicate independent viral transduction experiments. **P* < 0.01. (**D**) A metaphase FISH analysis was performed to assess *CD44* on HSR or DMs in the control GFP-KD (shCont) and RAD21-KD SNU16 cells (R#35) on day 60 after lentivial transduction. Chromosome-2 centromere (labeled with Cy3 for the control; white arrows) served as control. A schematic representation of the localization of the FISH probes specific for *CD44* (labeled with FITC; green) located at chromosome 11p13 is shown above. (**E**) The total numbers per cell of DMs containing *CD44* were blindly counted in the control GFP-KD and RAD21-KD SNU16 cells on day 60 after lentivial transduction. Fifty mitotic spreads were evaluated per sample (± SD). Representative FISH images are shown in (**D**). **P* < 0.01.

5. Cohesin depletion reduces the enrichment of pre-replication complex at replication origins near amplified regions

DNA replication occurs in two steps: the licensing of origin of replication and the initiation of DNA replication [46-48]. Pre-replication complex (pre-RC) is responsible for proper recruitment of replication licensing machinery at replication origins [46, 47]. Interestingly, several pieces of evidence have suggested that perturbation of DNA replication initiation can eliminate the number of amplified genes on DMs in several human cancers [49, 50]. Thus, a regional DNA replication defect by improper recruitment of pre-RC may contribute to change the overall copy-number of amplified genes [4, 8, 48, 51]. Recently, cohesin has been shown to directly regulate DNA replication [39, 52]. Moreover, cohesin complexes are particularly enriched at replication origins during DNA replication [39, 53, 54]. Hence, it is of interest to determine whether cohesin depletion might affect the enrichment of pre-RC at replication origins near amplified genes.

First, we compared the binding of pre-RC to the *APIP/PDHX/CD44 locus* in CIN^+ SNU16 cells with a highly amplified *APIP/PDHX/CD44 locus* on HSRs and DMs and HCT116 cells having two copies of *APIP/PDHX/CD44*. Based on a DNA replication origin database (DeOri; http://tubic.tju.edu.cn/deori/), we identified four DNA replication origins near the *APIP/PDHX/CD44 locus* (Figure 4). Pre-RC is composed of several proteins, such as the origin recognition complex (ORC), six minichromosome maintenance subunits (MCM 2-7), CDC45, GINS tetramer, and DNA polymerases (Pol α, Pol ε, and Pol δ) [55-57]. Binding of Pol α, which is

required for eukaryotic DNA replication [58], at replication origins within the *APIP/PDHX/CD44* locus was strongly enriched in SNU16 cells (Figure 4A). In contrast, relatively low Pol α binding was detected in HCT116 cells. Each value was normalized with gene copy number to determine the correct signal per region (data not shown). Similarly, enrichment of MCM7, which forms a pre-RC to recruit the DNA polymerase complex to target origins and functions as a replicative DNA helicase [59, 60], in SNU16 cells was higher than in HCT116 cells. We also observed strong recruitment of CDC45, a well-known MCM helicase activator [60], at replication origins within the *APIP/PDHX/CD44* locus in SNU16 cells but not in HCT116 cells, suggesting a positive correlation between DNA copy number and the enrichment of pre-RC. We next found that strong binding of pre-RC was notably impaired in RAD21-KD SNU16 cells compared to control GFP-KD cells. Significantly fewer pre-RC was detected in RAD21-KD SNU16 cells at replication origins within the *APIP/PDHX/CD44* locus. Using immunofluorescence assays, we found that RAD21 depletion led to reduced co-localization of MCM7 and RAD21 (Figure 4C and D). However, reduction of cohesin by RAD21-KD did not change the basal mRNA expression of pre-RC [39]. Taken together, these results suggest that cohesin depletion reduces the enrichment of pre-RC at replication origins near amplified regions on HSRs and DMs. Thus, continuous reduction of active DNA-replication, which is essential for the maintenance of amplified genes on HSRs and DMs [7], by cohesin depletion might provoke copy-number loss of amplified oncogenes in CIN^+ SNU16 cancer cells [4, 8, 48].

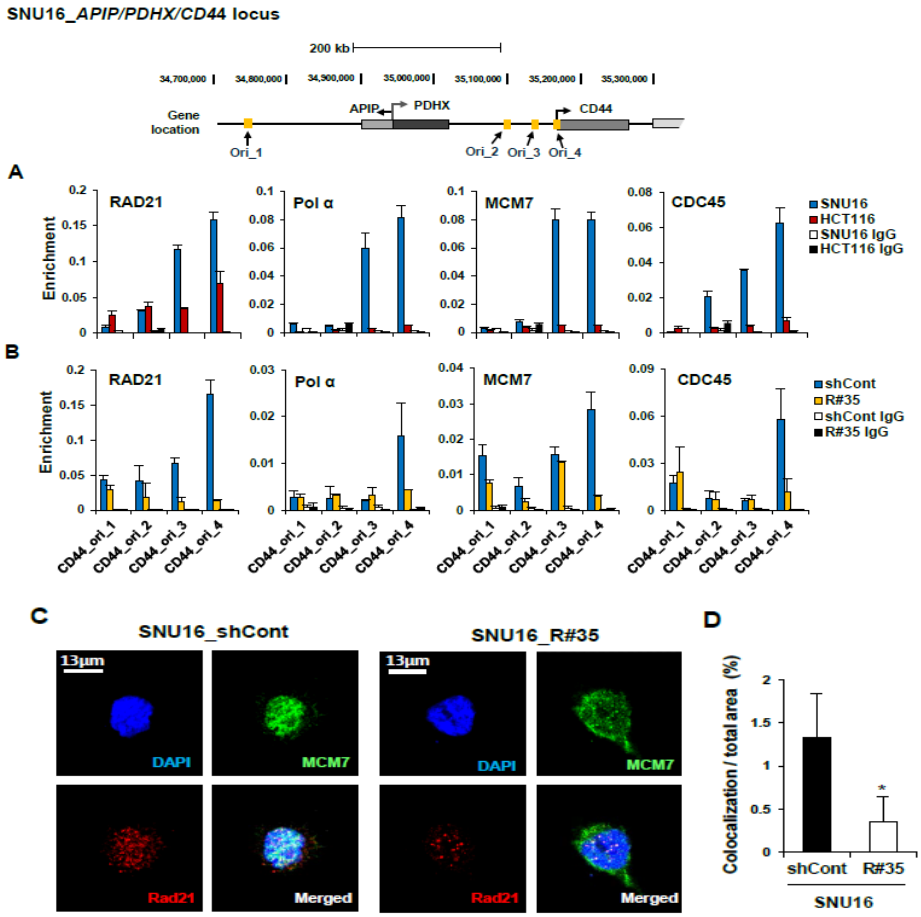

Figure 4. Down-regulation of cohesin impairs localization of pre-replication complex at replication origins within the amplified *APIP/PDHX/CD44* locus

(**A**) A ChIP assay was performed with SNU16 (blue bar) and HCT116 (red bar) cells using antibodies against RAD21, DNA polymerase α (Pol α), MCM7, and CDC45. The location of previously published replication origin sequences [45] near the *APIP/PDHX/CD44* locus used for qPCR are shown with names below. (Mean ± SEM, n = 3 biological replicates). (**B**) A ChIP assay was performed with control

GFP-KD (blue bar) or RAD21-KD SNU16 cells (R#35; yellow bar) on day 60 after lentivial transduction using antibodies against RAD21, Pol α, MCM7, and CDC45. (Mean ± SEM, n = 3 biological replicates). (**C**) Immunofluorescence staining of DNA (DAPI, blue), MCM7 (green), and RAD21 (red) in control GFP- KD (left panel) or RAD21-KD SNU16 cells (right panel). (**D**) Percentage of MCM7 and RAD21 co-localization in control GFP-KD (filled bar) or RAD21-KD SNU16 cells (unfilled bar) by unbiased automatic quantification [39]. Data are presented as averages ± SD of individual cells (n = 100). *$P < 0.01$; Student's *t* test.

6. Copy-numbers of amplified gene existing in both HSRs and DMs are decreased by cohesin reduction

Next, to further confirm that two different types of gene amplification, HSRs and DMs, could be affected by cohesin reduction, a CNV assay was performed with COLO 320-HSR and COLO 320-DM cells stably transfected with control GFP-shRNA or two different RAD21-shRNAs. COLO 320-HSR and COLO 320-DM cells are derived from human colon carcinoma and carry multiple copies of *c-Myc* localized in HSR and DMs, respectively [7]. By RAD21-KD in the COLO 320-HSR cells, we found that cohesin reduction induced copy-number loss of the highly amplified *c-Myc* without loss of HSR harboring *c-Myc* (Figure 5A-C). We similarly observed that RAD21-KD resulted in copy-number loss of the *c-Myc* localized in DMs in COLO 320-DM cells (Figure 6A-C), suggesting that down-regulation of

cohesin decreases the high-level *c-Myc* amplifications existing in both HSRs and DMs in cancer cells. We also found that RAD21-KD blocks the formation and enrichment of cohesin complex near the *c-Myc* in COLO 320-HSR and COLO 320-DM cells (Figure 5D and 6D). The *c-Myc* segment formed long-range chromatin interactions in both COLO 320-HSR and COLO 320-DM cells (blue line, Figure 5E and 6E). Down-regulation of cohesin by RAD21-KD resulted in the release of spatial chromatin organization of the *c-Myc* in COLO 320-HSR and COLO 320-DM cells (red line, Figure 5E and 6E), resulting in a striking reduction in *c-Myc* expression (Figure 5F and 6F). We also found that the binding of Pol α, CDC45, and MCM7 at replication origins near c-Myc were diminished by RAD21-KD in COLO 320-HSR and COLO 320-DM (Figures 5G and 6G). Collectively, we demonstrated that cohesin reduction via RAD21-KD decreases the expression and the focal copy-number of amplified genes existing on both HSR and DMs in CIN^+ cancer cells, thereby maintaining low expression levels of previously highly amplified genes.

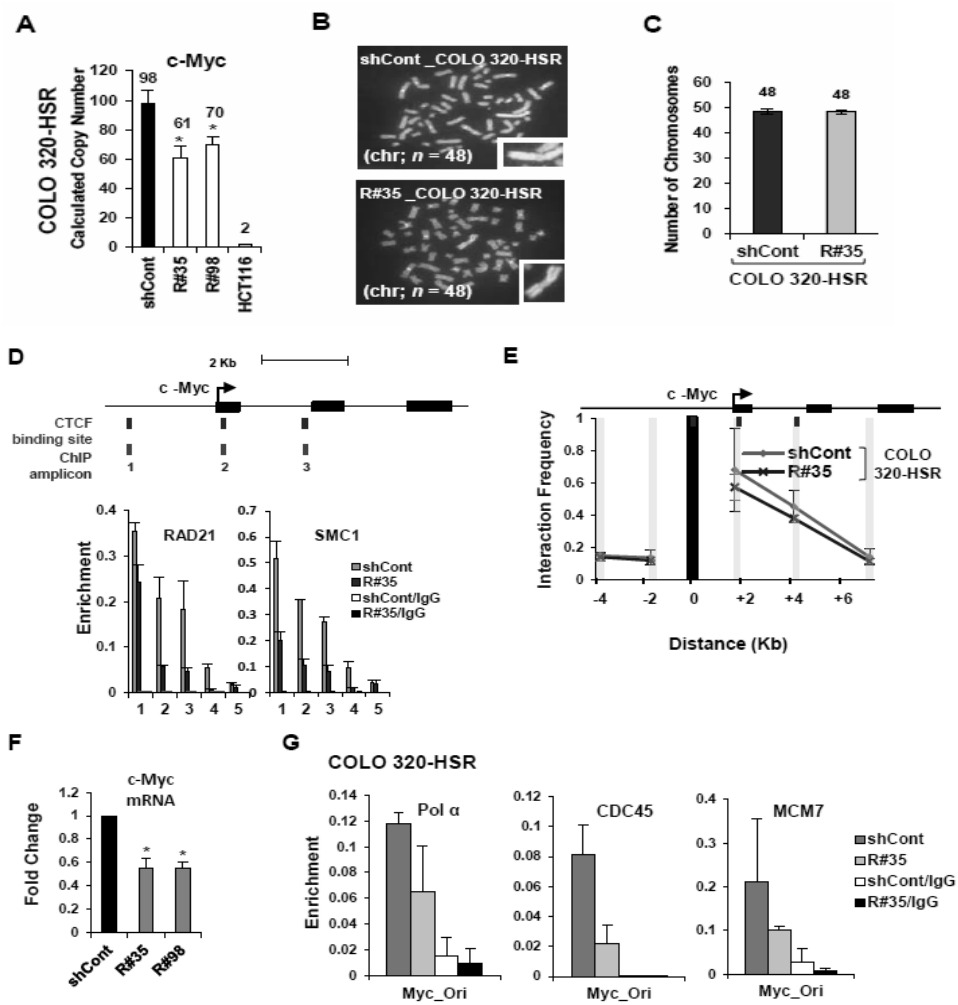

Figure 5. Copy-numbers of amplified gene existing in HSRs are decreased by cohesin reduction

(**A**) COLO 320-HSR cells were stably transduced with control GFP-shRNA or two different Rad21-shRNAs (R#35 and R#98). Changes in copy-numbers of the *c-Myc* were quantified using a TaqMan quantitative PCR-based CNV assay. The average of three viral transduction experiments ± SD is presented. **P* < 0.01. (**B**) Metaphase

FISH analysis with *c-Myc* (labeled with FITC; green) and chromosome 2 centromere (labeled with Cy3 for the control; red) revealed a reduction of *c-Myc* located within HSR in RAD21-KD COLO 320-HSR cells. Notably, amplified *c-Myc* exists as HSR and inverted repeats within the chromosome of the COLO 320-HSR cells. (**C**) Total chromosome numbers of the control GFP-KD or RAD21-KD COLO 320-HSR cells were counted after treatment with nocodazol. Fifty mitotic spreads were evaluated for each sample (± SD). (**D**) A ChIP was performed with antibodies to Rad21 and SMC1 in control GFP-KD (blue bar) or RAD21-KD COLO 320-HSR (red bar). (Mean ± SEM, n = 3). *c-Myc* at chromosome 8q24 are illustrated to scale. The location of putative CTCF/Rad21 binding sites and primer pairs used for qPCR are shown with names below. 3'HS1 of the human *β-globin* locus (amplicon 4) and *Necdin* (amplicon 5) served as controls. (**E**) 3C assay of *c-Myc* in COLO 320-HSR cells after RAD21-KD. DpnII restriction sites in *c-Myc* appear as gray shaded bars. Black shading indicates the anchor fragment of the 5' CTCF binding sites of *c-Myc*. (Mean ± SEM, n = 3 biological replicates). (**F**) The expression of *c-Myc* was measured by qRT-PCR on day 60 after RAD21-KD in COLO 320-HSR cells. Each value was normalized to that of 18S ribosomal RNA relative to the control GFP-KD cells. The average of biological triplicate independent viral transduction experiments ± SD is presented. **P* < 0.01. (**G**) A ChIP assay using previously published replication origin sequences near the *c-Myc* locus [45] was performed with antibodies against Pol α, CDC45, and MCM7 in control GFP-KD or RAD21-KD COLO 320-HSR cells on day 60 after lentivial transduction. (Mean ± SEM, n = 3 biological replicates).

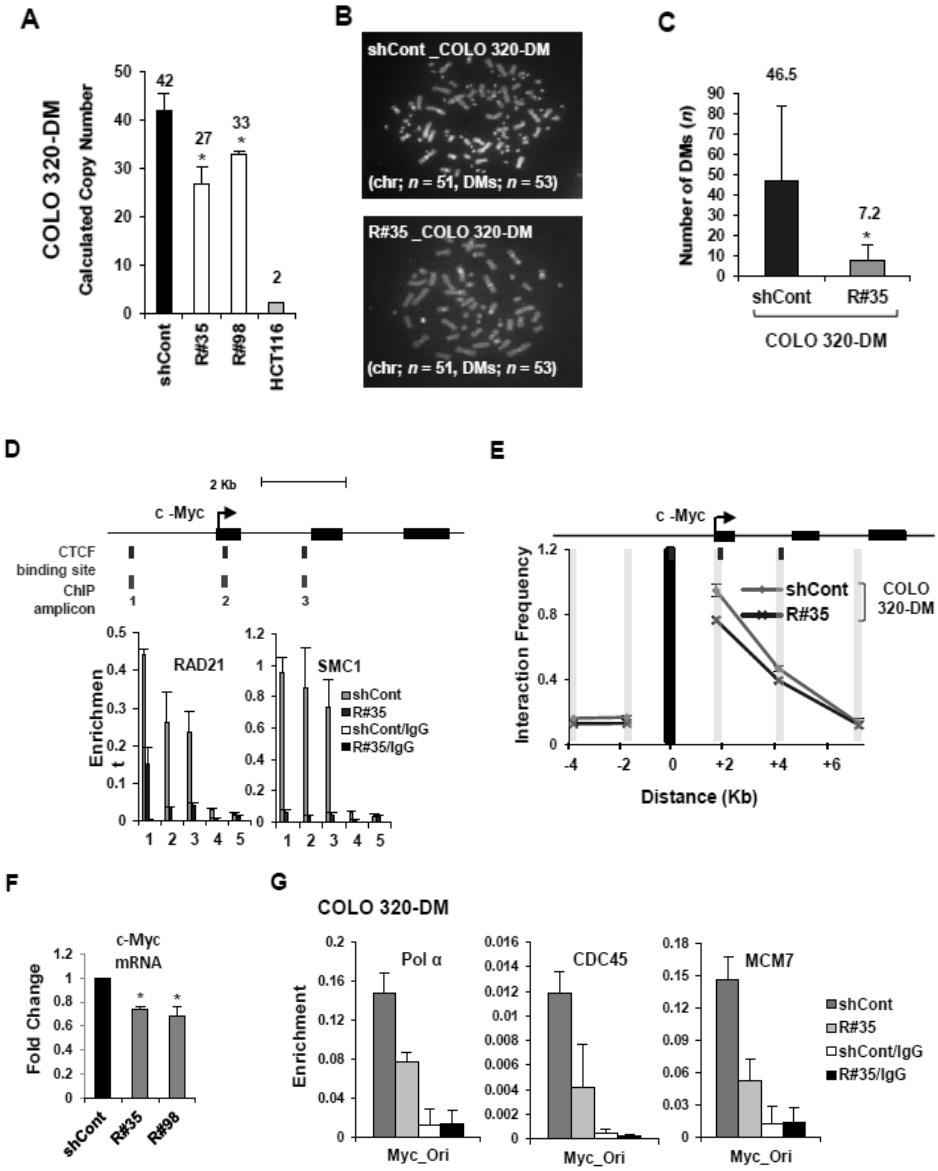

Figure 6. Copy-numbers of amplified gene existing in DMs are decreased by cohesin reduction. (**A**) COLO 320-DM cells were stably transduced with control GFP-shRNA or two different Rad21-shRNAs (R#35 and R#98). Changes in copy-numbers of the *c-Myc* were quantified using a TaqMan quantitative PCR-based CNV

assay. The average of three viral transduction experiments ± SD is presented. *P < 0.01. (**B**) Metaphase FISH analysis with *c-Myc* (labeled with FITC; green) and chromosome 2 centromere (labeled with Cy3 for the control; red) revealed a reduction of *c-Myc* located within DMs in RAD21-KD COLO 320-DM cells.

(**C**) Total numbers of DMs per cell were blindly counted in control GFP-KD and RAD21-KD COLO 320-DM cells. (Mean ± SD, n = 50). *P < 0.01. (**D**) A ChIP was performed with antibodies to RAD21 and SMC1 in control GFP-KD (blue bar) or RAD21-KD COLO 320-DM (red bar). (Mean ± SEM, n = 3 biological replicates). 3'HS1 of the human *β-globin* locus (amplicon 4) and *Necdin* (amplicon 5) served as controls. (**E**) 3C assay of *c-Myc* in COLO 320-DM cells after RAD21-KD. DpnII restriction sites in *c-Myc* appear as gray shaded bars. Black shading indicates the anchor fragment of the 5' CTCF binding sites of *c-Myc*. (Mean ± SEM, n = 3 biological replicates). (**F**) The expression of *c-Myc* was measured by qRT-PCR on day 60 after RAD21-KD in COLO 320-DM cells. Each value was normalized to that of 18S ribosomal RNA relative to the control GFP-shRNA expressing cells. The average of triplicate independent viral transduction experiments ± SD is presented. *P < 0.01. (**G**) A ChIP assay using previously published replication origin sequences near the *c-Myc* locus [45] was performed with antibodies against Pol α, CDC45, and MCM7 in control GFP-KD or RAD21-KD COLO 320-DM cells on day 60 after lentiviral transduction. (Mean ± SEM, n = 3 biological replicates).

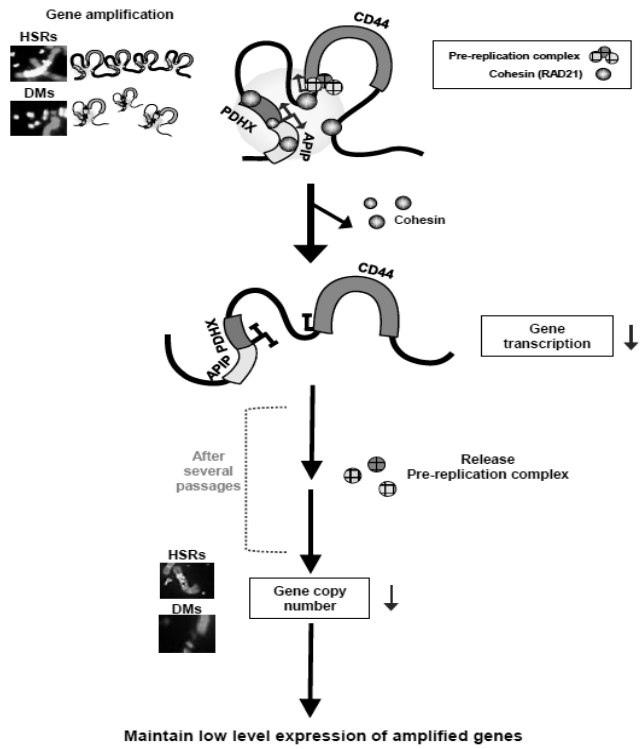

Figure 7. Proposed model for cohesin-mediated copy-number loss of highly amplified genes existing on DMs and HSRs in human cancer cells

APIP/PDHX/CD44 locus located in HSRs and DMs forms spatial chromatin organizations in SNU16 cells. Cohesin appeared to stabilize long-range chromatin interactions through direct interactions among CTCF/cohesin localization sites. Down-regulation of cohesin by RAD21-KD abolished the proximity between CTCF/Rad21 binding sites within these segments, thereby reducing *APIP/PDHX/CD44* expression. After several passages, RAD21-KD decreases the enrichment of pre-RC at replication origins near these regions, result in reducing the copy numbers of amplified genes existing in HSRs and/or DMs in cancer cells. See text for more details.

DISCUSSION

Cohesin is required to form sister chromatid cohesion for proper chromosome segregation during mitosis and meiosis [13]. Therefore, defects in chromosomal segregation caused by inactivating mutations of chromatid cohesion genes leading to increased chromosomal instability and aneuploidy have been identified in human cancer [16, 61]. Although a high frequency of recurrent mutations and deletions of cohesin components has been found in various types of human cancer [16, 62, 63], such genetic alternations in genes encoding the cohesin components seem to be very rare in our human gastric cancer samples (data not shown). Instead, aberrant over-expression of cohesin components is frequently observed in human gastric cancer (15 out of the 24 samples, 62.5%). We also tested the human gastric cancer dataset with 50 tumor and normal pairs from the Cancer Genome Atlas (TCGA) database and obtained similar results. This suggests the possibility that elevated cohesin level may generally affect tumorigenesis through alternative mechanisms other than the induction of sister chromatid cohesion defects in human gastric cancer.

Since human gastric cancers show a high level of gene amplification [27, 29, 64], we therefore wondered if elevated cohesin level is required to maintain gene amplification. In the current study, we found that cohesin reduction decreases the focal copy-number of amplified *APIP/PDHX/CD44* segments on HSRs and DMs in SNU16 cells. Using COLO 320-HSR and COLO 320-DM cells, we also confirmed that down-regulation of cohesin enrichment can generate the copy-number loss of amplified *c-Myc* existing on both HSRs and DMs. Considering the fact that our

RAD21-KD cells proliferated well without developing defective sister chromatid cohesion formation or aberrant chromosome segregation during mitosis and meiosis (Figure 1), cohesin-mediated copy-number alterations might be independent of mitotic defects or chromosomal missegregation [65, 66]. To extend the generality of our observations demonstrating the effects of cohesin reduction, we tested the highly amplified *WDR11-AS1/WDR11* locus in RAD21-KD SNU16 cells and obtained the same results. In addition, we observed very similar results after RAD21-KD in N87 gastric cancer cells with *HER2* amplification. However, copy-number changes of the same set of genes were not detected following RAD21-KD in near-diploid HCT116, LoVo and HepG2 cells. Therefore, cohesin-mediated copy-number loss of highly amplified genes on HSRs and DMs may be not a general characteristic of cells with stable chromosomes but is instead specific to cancer cells with multiple structural chromosomal changes.

Although the nature of gene amplification in human cancer is not fully understood yet, in general, gene amplification resided on the DMs or HSR occurs and is maintained by DNA replication initiation during tumorigenesis [4, 7, 46, 47]. Since the DMs are autonomously replicating extrachromosomal genetic elements [4, 7], repeated rounds of replication initiation of the DMs may be required for efficient gene amplification [7]. Therefore, disruption of DNA replication initiation by treatment of DNA replication inhibitors such as hydroxyurea or ionizing radiation can eliminate the number of amplified genes on DMs in human cancers [7, 49, 50]. Furthermore, because DMs can be generated from the repeated BFB cycle triggered by DSBs of HSR [67], failure to maintain DMs by down-regulating cohesin

molecules may also reduce gene amplification resided on the HSR. In this study, we found that cohesin and pre-RC are highly enriched at replication origins near amplified genes. Cohesin depletion resulted in a reduced recruitment of pre-RC such as Pol α, CDC45, and MCM7 (Figure 4). This result suggests that deregulating DNA replication initiation by cohesin reduction might generate a regional replication defect by perturbing proper recruitment of replication licensing machinery, subsequently changing the overall copy number of amplified genes resided on the DMs or HSR [4, 8, 48, 51].

Highly amplified *APIP/PDHX/CD44*, *WDR11-AS1/WDR11*, and *c-Myc* in SNU16 cells are either directly or indirectly linked to tumor progression and chemosensitivity [68-70]. Down-regulation of cohesin by RAD21-KD enhanced the anti-proliferative effects of DNA-damaging agents, cisplatin or PARP inhibitor, in SNU16 and N87 cancer cells, consistent with earlier data [24, 25]. In the case of HCT116, LoVo, and HepG2 cancer cells with stable chromosome, however, no significant effect was observed following treatment with DNA-damaging agents. Thus, the copy-number loss of oncogenic genes might sensitize cancer cells to DNA-damaging anti-cancer drugs [68]. Given that gene amplification is associated with drug resistance and an unfavorable prognosis [4], the regulation of gene amplification by down-regulation of elevated cohesin component holds promise as a therapeutic strategy for treating cancer with genomic instability.

In summary, we have shown that down-regulation of elevated cohesin by RAD21-KD disrupts the cohesin-mediated chromatin structure and the enrichment of pre-RC

at replication origins near the amplified regions existing in both HSRs and DMs, resulting in reducing the copy numbers of amplified genes in human cancer cells. Thus, cohesin is essential to stabilize high-level gene amplification in cancer cells with genomic instability. These results highlighted the importance of the elevated cohesin level in the formation of genomic instability in human cancer.

Ⅱ. Disruption of intrachromosomal interactions by deficient cohesin initiate epithelial-mesenchymal transition and stemness in cancer

ABSTRACT

EMT-MET process is a reversible event in tumorigenesis controlled by complex networks though, their cue that activates EMT-initiating factor and the mechanism how EMT-MET occurs reversibly are very little known. We found that cohesin-mediated chromatin architecture, a cue for EMT activation, participates in tumor metastasis. Depending on RAD21 mRNA stability, mesenchymal cancer with low level of RAD21 have a shorter mRNA half-life than epithelial cancer with high level of RAD21. A deprivation of RAD21 in epithelial cancer caused a rapid transcriptional induction of TGFB1 and ITGA5 which directly led to a cellular transition into mesenchymal feature. Insufficient binding of RAD21 on the genes significantly released the intrachromosomal interactions in each gene, causing the active recruitment of transcription factors. Finally, cancer stem-like cells (CSCLs) have weaker binding of cohesin, and thus, the chromatin in TGFB1 and ITGA5 were loosened compared to parental cells. These findings indicate that cohesin-mediated three dimensional chromatin structures are responsible for the initiation and regulation of EMT plasticity in a small population of tumors or cancer stem cell model.

Key words : EMT, cohesin, higher-order chromatin structure, cancer stem cell

INTRODUCTION

Around 90% of human cancer cases is caused by metastasis [1], a multi-step process in which primary tumor cells disseminate from their origin site and move into secondary locations to acquire a better environment for tumor proliferation [2, 3]. Epithelial-mesenchymal transition (EMT) associated with metastasis is known as an initiation process related to intravasation [4, 5]. During EMT, epithelial cancer cells acquire migratory potential, loss of apical-basal polarity, and resistance to apoptotic stimuli that promote detachment from the origin sites and neighboring cells through coordinate gain of EMT-related genes and loss of epithelial-related genes expression. Consequently, the cancer cells gradually obtain migratory and invasive capabilities [6]. According to the cancer stem cell (CSC) hypothesis, tumor growth is driven by only subpopulation of tumor-initiating cells that have self-renewal and multi-potency properties [7]. It is known that CSCs have mesenchymal traits and are capable of mobility and proposed as the seeds of metastasis [7]. Additionally, CSC plasticity postulates that cancer has CSCs and non-CSCs, and these different cancer cells character bidirectional conversion. Metastasis in patients with aggressive forms of cancer and CSCs are closely linked to cancer mortality. Understanding the regulation mechanisms of EMT and mesenchymal to epithelial transition (MET), a reversible process of EMT, are thus important for preventing tumor metastasis [8]. During cancer metastasis, the EMT-MET is essential for the timely and accurate differentiation of epithelial (or mesenchymal) cancer cells into mesenchymal (or epithelial) cancer cells for tumor development [9]. Over the past decades, many

groups have studied EMT and EMT-related genes such as E-cadherin (*CDH1*), vimentin (*VIM*), Tumor growth factor β (*TGFB*), Twist-related protein 1 (*TWIST1*), β-catenin (*CTNNB1)*, Zinc finger E-box-binding homeobox 1/2 (ZEB1/2), and the miR200 family [10]. Recent studies have provided compelling evidence for epigenetic regulation of the EMT process including histone deacetylation and DNA methylation of CDH1, expression of non-coding RNA (mir-200 a,b,c, mir-429, and mir-141) that regulates EMT plasticity, and post-translational modifications such as sumoylation of ZEB2, and phosphorylation of snail family zinc finger 1 (SNAI1) [11-14]. Based on these findings, epigenetic mechanisms appear to play a crucial role in the regulation of EMT-related genes and are important mechanical factors during the EMT process. Despite these data elucidating various factors that control dramatic changes during EMT, the upstream regulatory molecules responsible for initiating EMT, called "cues", are still unclear [7].

Higher-order chromatin architecture is known to be important for gene regulation during hematopoiesis, erythropoiesis, and development. Therefore, chromatin architectural proteins such as CCCTC-Binding Factor (CTCF), cohesin, and LIM Domain Binding 1 (LDB1) have been actively studied [15, 16]. In particular, the cohesin complex, consisting of four main subunits, two SMC molecules (SMC1 and SMC3), STAG, and RAD21, tightly and dynamically controls genomic organization to regulate gene transcription, transcript splicing, chromosomal instability, and gene amplification in cancer [17, 18]. Substantial evidence has shown that cohesin proteins are involved in tumorigenesis. While cohesin complex is overexpressed and mutated in some types of cancer such as breast, prostate, and

colon, other malignancies such as oral squamous cell carcinoma, colorectal cancer, and myeloid leukemia express low levels or mutated forms of these proteins [19, 20]. It has been reported that RAD21, a subunit of cohesin complex, are expressed at a low level in metastatic breast and oral squamous cancers [21, 22]. However, the reason why the RAD21 are lower in metastatic than in epithelial cancer is still unclear. Although many distinct molecular mechanisms associated with the EMT process in cancer have been identified, the contributions of higher-order chromatin architecture to regulating EMT regulation and acquisition of mesenchymal traits are still unknown [23].

In the present investigation, we showed that deprivation of RAD21 in epithelial cancer cells increases the transcription of two EMT-related genes: TGFB1 and ITGA5 by releasing the higher-order chromatin structure of the genes. Up-regulation of these genes directly leads to EMT. Furthermore, this result is proven by the same outcomes in cancer stem-cell like cells (CSLCs) which was known to have mesenchymal traits. Results from our study strongly suggest that cohesin influences a reversible transition between epithelial and mesenchymal states in a subpopulation of cancer by dynamically regulating the expression of key genes responsible for EMT initiation by affecting the three-dimensional chromatin architectures.

MATERIALS AND METHODS

1. Cell culture, virus production, and transduction

Cells cultured in RPMI 1640 or DMEM supplemented with 10% fetal bovine serum (FBS), and gentamicin (10 μg/mL) [24] at 37°C in a humidified 5% CO_2 atmosphere. Control and RAD21-directed TRC lentiviral shRNAs were purchased from Open Biosystems. CSCL MDA-MB453 cells were obtained from the University of Pittsburgh Medical Center [25, 26]. Lentiviruses were produced by transducing 293FT cells with shRNA using a Virapower packaging mix (Invitrogen) as previously described [27]. The viruses were harvested from the media on day 3 by centrifugation, and cells were then incubated with viral supernatant in the presence of 6 μg/mL polybrene (Sigma). After 2 days of incubation, the transduced cells were cultured in the presence of 1 μg/mL puromycin (Sigma) for another 3 days before collection as previously described [16]. The knockdown efficacy was confirmed by qPCR and western blot analysis. To generate a stable knocked-down clone, several single colonies were isolated and independently expanded in the presence of puromycin as previously described [27].

2. Reverse transcription and Western blot analysis

Two μg total RNA was reverse transcribed with random hexamers as previously described [28]. Whole cell extracts were prepared, and western blot analysis was performed as previously described [29].

3. mRNA stability assay

Cells were treated with 10 μg/mL actinomycin D (mRNA decay) and harvested at indicated time points (0, 3, 6, 9, 12, and 24 hours). Total RNA was isolated by Trizol and DNase-treated for the analysis of RAD21 and c-Myc mRNA levels. Changes in RAD21 or c-Myc mRNA levels were determined by the $\Delta\Delta C_t$ method using 18S rRNAs for internal cross-normalization. All data were analyzed from at least three independent experiments, and statistical significance was validated by Student's *t*-testing.

4. Immunofluorecsence analysis

Cells expressing control and RAD21 (R#1) shRNAs were seeded on 0.01% poly-L-lysine (Sigma-Aldrich)–coated coverslips. Next day, the coverslips were rinsed once in PBS (37°C), fixed in 4% formaldehyde for 15 minutes, permeabilized with 0.5% Triton X-100 for 5 minutes, and then incubated with primary antibody for 1 hours at RT. The primary antibodies used in this study were mouse polyclonal anti-E-cadherin, anti-vimentin, anti-β-catenin, and anti-RAD21 (SC-8426, SC-6260, SC-7963 from Santa Cruz Biotechnology, and ab992 from Millipore, respectively) at a dilution of 1:100. The coverslips were rinsed 3 times with PBS, followed by incubation with the appropriate fluorophore-conjugated secondary antibody (Invitrogen) for 1 hr at RT. The cells were counterstained with 4′,6-diamidino-2-phenylindole (DAPI; 300

nmol/L; Invitrogen) and the coverslips were mounted on slides using Faramount aqueous mounting medium (DAKO).

5. Affymetrix Whole transcript Expression Arrays

Total RNA was extracted from MCF7 or SNU16 cells expressing Control and RAD21 (R#1) shRNAs (Day 30) using an RNease mini kit (Qiagen, Valencia, CA, USA) in accordance with the manufacturer's instructions. The Affymetrix Whole transcript Expression array process was executed according to the manufacturer's protocol (GeneChip Whole Transcript PLUS reagent Kit). cDNA was synthesized using the GeneChip WT (Whole Transcript) Amplification kit as described by the manufacturer. The sense cDNA was then fragmented and biotin-labeled with TdT (terminal deoxynucleotidyl transferase) using the GeneChip WT Terminal labeling kit. Approximately 5.5 μg of labeled DNA target was hybridized to the Affymetrix GeneChip Human 2.0 ST Array at 45°C for 16 h. Hybridized arrays were washed and stained on a GeneChip Fluidics Station 450 and scanned on a GCS3000 Scanner (Affymetrix). Signal values were computed using the Affymetrix® GeneChip™ Command Console software.

6. Chromatin immunoprecipitation (ChIP) assay and quantitative real-time PCR (qPCR)

ChIP assays were performed as previously described [27]. qPCR using SYBR Green

(Molecular Probes) was performed to observe enriched DNA or cDNA using StepOnePlus (Applied Biosystems) as previously described [28]. The enrichment of target DNA over the input was calculated using the ΔΔCt method, and the results were presented as the mean ± SEM [16]. The PCR primers used for the ChIP and qPCR assays are available upon request.

7. Chromosome conformation capture (3C) assay

A 3C assay was performed as previously described [27, 30, 31] with minor modification. Briefly, chromatin crosslinked in 1 % formaldehyde was digested with 1000 U of the restriction enzymes (NEB) overnight followed by ligation with 2000 U of T4 DNA ligase (NEB) at 16°C for 4 h. Crosslinking was reversed, and the DNA was then purified by phenol extraction and ethanol precipitation as previously described [27]. To generate control templates for the positive controls, equimolar amounts of the BAC clones were digested with 200 U of the restriction enzymes overnight at 37°C as previously described [32]. After phenol extraction and ethanol precipitation, DNA fragments (200 ng/μL) were ligated with T4 DNA ligase. Digestion efficiency was calculated as previously described [33] and samples with efficiencies greater than 90 % were used for the 3C assays. Crosslinking frequency and ligation efficiencies between different samples were normalized relative to the ligation frequency of two adjacent the restriction enzyme fragments in the *ERCC3* gene [33]. Quantitation of the data was performed by qPCR using SYBR Green (Molecular Probe).

8. Wound-healing assay

Cells were seeded at a high density on 60-mm culture dishes. Twelve hours later, the wounds were made by scraping through the cell monolayer with a pipette tip. After washing with PBS, the cells were incubated in growth medium and observed at 0, 24, and 48 h under a microscope. The wound closure was estimated as the ratio of the reaming wound area relative to the initial wounded area [34].

9. Antibodies

Antibodies specific for the following factors were used in this study: E-cadherin (SC-8426), vimentin (SC-6260), β-catenin (SC-7963), normal rabbit IgG (SC-2027), TGFBR (SC-399), TGFBR (SC-1700), and RNA pol II (SC-899) from Santa Cruz Biotechnology; RAD21 (ab992) from AbCam Anti-AcH3 (#06-599) from Millipore; α-tubulin (T1568) from Sigma. Anti-ITGA5 antibody (BD51-9001996) was purchased from BD bioscience.

10. Statistical Methodologies

Statistical tests were applied as indicated in figure legends. Asterisks are as follows: *$P < 0.01$ and **$P < 0.05$.

RESULTS

1. RAD21 expression in mesenchymal breast cancer is relatively lower than that of epithelial cells

RAD21 was previously demonstrated to be low-expressed in metastatic cancer cells such as breast and oral squamous cell carcinoma [21, 22]. We wondered whether RAD21 might be important in determining the state of either EMT or MET. We therefore compared RAD21 expressions between epithelial (HCC70, T47D, and MCF7) and highly metastatic breast cancer cell lines (MDA-MB-231, HCC1143, and MDA-MB-157) [35] (Figure 1A). Consistent with the previous studies, we observed a relatively low-expression of RAD21 protein in mesenchymal breast cancer cell lines compared with epithelial breast cancer cell lines. Next, to visually compare the relationships between RAD21 expression and EMT state, we analyzed Immunofluorescence staining with RAD21 and E-cadherin, a well-known epithelial marker, or VIM, a marker for mesenchymal trait, in MCF7 or HCC1143 cells. Consistent with the Western blot data, we observed that HCC1143 cells expressed a high level of VIM and low levels of E-cadherin and RAD21 while MCF7 cells had a low level of VIM and high levels of E-cadherin and RAD21 (Figure 1B). To understand why different levels of RAD21 protein expression were observed when comparing mesenchymal and epithelial breast cancer cells, we analyzed RAD21 mRNA (Figure 1C). No significant difference in mRNA expression was observed between the cells. We then assessed RAD21 expression in epithelial breast cancer

MCF7 cells- and mesenchymal breast cancer HCC1143 cells- following treatment with 10 μg/mL actinomycin D (Act D) for 0, 3, 6, 9, 12, and 24 h (Figure 1D). The levels of RAD21 transcripts and protein in MCF7 cells remained steady after 24 h of Act D treatment. In contrast, a dramatic reduction of RAD21 transcripts and protein were observed after 6 h of Act D exposure in HCC1143 cells. We also observed a significant reduction of c-Myc transcripts, which was used as a control [36, 37] in both cell lines (Figure 1D). These findings showed that low expression of RAD21 protein in mesenchymal breast cancer cell lines might be due to less stable transcripts than those in epithelial cell lines with higher RAD21 expression.

Taken together, our results demonstrated that the stability of RAD21 transcripts in mesenchymal breast cancer cell lines was relatively low compared to those in epithelial cell lines, thus leading to a low expression of RAD21 in mesenchymal breast cancer cells.

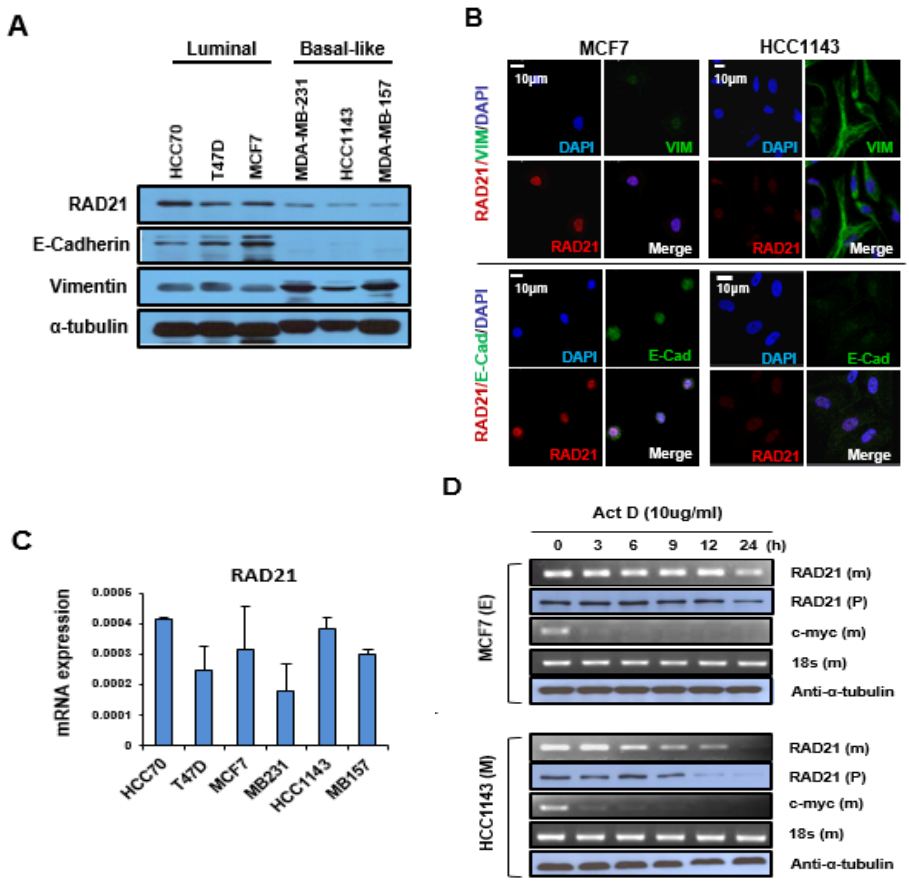

Figure 1. Unstable RAD21 mRNA leads to low level of RAD21 protein in Mesenchymal breast cancer cells.

(A) Results of a Western blot analysis of RAD21, E-cadherin, and VIM are shown for luminal and basal-like breast cancer cell lines. **(B)** The level of RAD21 mRNA in breast cancer cell lines. Values were normalized relative to 18S transcription. The plotted data are the average for three independent experiments. Bars represent the mean ± SD. **P* < 0.01 and; ***P* < 0.05. **(C)** Immunofluorescence staining for VIM (green) or E-cadherin (green) and RAD21 (red) in a panel of MCF7 or HCC1143

cells. **(D)** Stabilities of the RAD21 transcript and protein in MCF7 or HCC1143 cells. The cells were treated with 10 μg/mL actinomycin D for 0, 3, 6, 9, 12, and 24 h, after which total RNA and proteins were extracted. c-Myc and 18S were used as thecontrols. (m: mRNA, P: protein).

2. Disruption of RAD21 expression in epithelial cancer cells induces transcription of two EMT-related genes: TGFB1 and ITGA5

Since we found that RAD21 expression levels correspond to the EMT state (Figure 1A), we questioned whether RAD21 was critical for determining the fate of cellular EMT state in cancer. We therefore stably knocked down (KD) RAD21 expression using RAD21-specific shRNA (shR#1 and shR#2) in epithelial breast MCF7 and T47D cells and gastric cancer SNU16 and SNU620 cells (Figure 2A). Interestingly, sufficient knockdown of RAD21 in the cells significantly decreased E-cadherin levels and simultaneously induced VIM expression (Figure 2B). We also evaluated the expression of mesenchymal markers such as ZEB1, ZEB2, N-cadherin (CDH2), fibronectin (FN), TWIST, and SNAIL2 (Slug) [38] to confirm the induction of EMT by RAD21 depletion in MCF7 and SNU16 cells (Figure 2C). As shown in Figure 2C, the expression of most EMT markers was significantly increased in the

Rad21-Knockdown (RAD21KD) cells although the expression of all EMT markers was not simultaneously induced in both types of cells. Based on these results, we hypothesized that RAD21 tightly regulates EMT plasticity in cancer cells. To identify the target genes of RAD21 which trigger EMT, we analyzed microarray data by comparing shControl (shCont) and RAD21KD (shR#1) in MCF7, and SNU16 cells (Figure 2D). Among the genes up-regulated more than two-fold by suppressing RAD21 expression, we found that TGFB1 and ITGA5 mRNA levels were increased in both RAD21KD-MCF7 and RAD21KD-SNU16 cells (Figures 2D and 3D). According to many other studies on EMT, TGFB1 has been known as a key regulator of EMT in cancer progression, development, and fibrosis [39, 40]. *In vitro* studies have shown that treating various epithelial cells with TGFB1 initiates EMT [40, 41] and it was reported that TGFB1 cross-talks with other pathways to lead to EMT, especially ITGA5 [42]. ITGA5 encodes the integrin alpha-5 chain and forms a hetero-dimeric chain with one of various beta chains to form intergrins, which act as receptors and transport environmental signals to cells by binding to the extracellular matrix (ECM) proteins [43]. A previous study showed that during the EMT process ITGA5 expression is induced in transformed epithelial cells [44]. To confirm the microarray data, we measured the mRNA expression of TGFB1 and ITGA5 in RAD21KD-MCF7, -T47D, -SNU16 and -SNU620 cells (Figure 2E). Consistent with the microarray data, quantitative real-time PCR (qPCR) results showed that both TGFB1 and ITGA5 mRNA expression was induced in RAD21-depleted epithelial cells. We wondered if this result was simply an effect of RAD21 deprivation in epithelial cells or if it was an outcome of long-term stable RAD21 knockdown using

lentiviral-shRNA vectors. To address this question, we transiently depleted RAD21 mRNA using RAD21-specific siRNA. Though the induction of TGFB1 and ITGA5 expression was more modest compared to stable knockdown of RAD21 (shown in Figure 2E), we observed an increase of TGFB1 and ITGA5 mRNA following transient RAD21 depletion. TGFB1 and ITGA5 expression was induced along with transcription changes of EMT-related genes in RAD21KD epithelial cancer cells. These two factors were highly expressed in mesenchymal breast cancer cells compared to epithelial breast cancer cell lines (Figure 2F). To next determine which gene was more susceptible or responded more rapidly to RAD21KD, we transiently depleted RAD21 in a time-dependent manner using siRNA. ITGA5 transcription was induced in the cells 12 h after transfection and the induced level last over 48 h. After the induction of ITGA5 expression, TGFB1 mRNA levels increased only after 48 h siRAD21 transfection, suggesting that ITGA5 was more sensitive to changes of RAD21 levels than TGFB1.

Taken together, our results indicated that RAD21 depletion in epithelial cancer cells led to a notable induction of EMT markers expression along with increased ITGA5 and TGFB1 transcriptions.

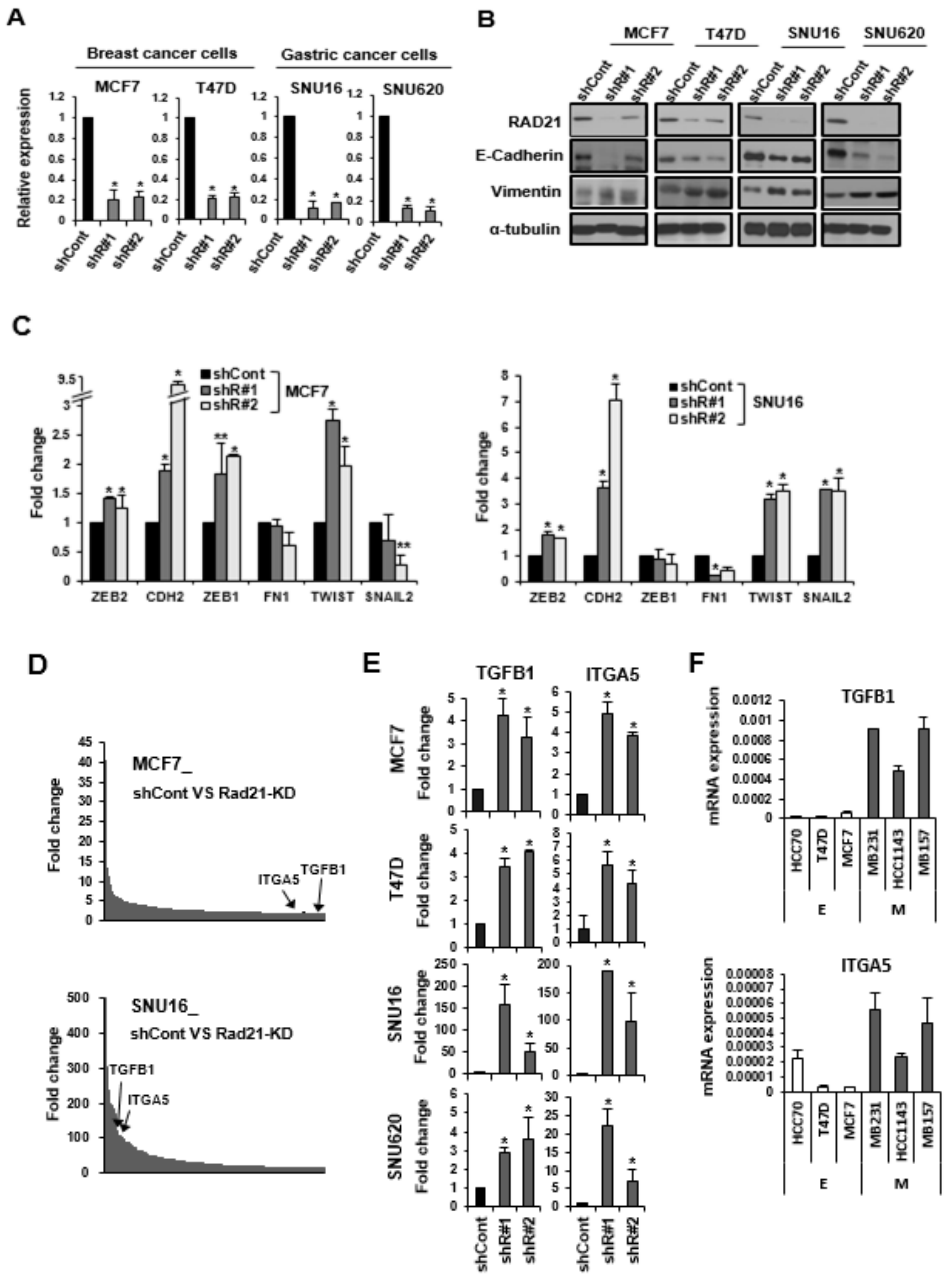

Figure 2. Reduction of RAD21 induces TGFB1 and ITGA5 transcription. (A)

The indicated cells were stably transduced with control GFP-shRNA or two different

RAD21-specific shRNA (shR#1 or shR#2, day 30). Data are presented as the mean ± s.d. for three independent experiments *$P < 0.01$ and; **$P < 0.05$. **(B)** Results of the Western blot analysis for RAD21, E-cadherin, and VIM in RAD21KD- MCF7, -T47D, -SNU16, and -SNU620 cells are presented. **(C)** qPCR was performed to measure the expression of EMT markers ZEB2, CDH2, ZEB1, FN1, TWIST, and SNAIL2 in RAD21KD-MCF7 or -SNU16 cells. Data are presented as the mean ± s.d. for three independent experiments *$P < 0.01$ and; **$P < 0.05$. **(D)** Fold changes in the expression of 2% of increased genes, each of which showed more than 2-fold upregulation in RAD21KD (shR#1) cells compared to the shCont. **(E)** Induction of TGFB1 and ITGA5 transcription in RAD21KD-MCF7, -T47D, -SNU16, and -SNU620 cells was evaluated using qPCR. Data are presented as the mean ± s.d. for three independent experiments *$P < 0.01$. **(F)** Expression of TGFB1 and ITGA5 mRNA normalized to the 18S transcript in luminal and basal-like breast cancer cell lines, E: epithelial-like, M: mesenchymal-like breast cancer cell lines.

3. Induced TGFB1 and ITGA5 expression leads directly to cellular morphological changes and acquisition of mesenchymal properties in RAD21-depleted cells.

Because EMT is known to acquire the ability of cell movement, it can take place when the cell has undergone morphogenesis [23]. As mentioned above, *In vitro* experiments showed that treating different epithelial cells with TGFB1 promotes the acquisition of a clear fibroblast-like phenotype characterized by a loss of epithelial traits and gain of mesenchymal features [42]. Additionally, ITGA5 knockdown also conferred an epithelial phenotype [45]. This led to the question whether TGFB1 and ITGA5 expression induced by RAD21KD in epithelial cancer cells cause cellular or morphological conversion into and EMT-like phenotype with an elongated spindle shape. To address this issue, we first observed changes of RAD21KD cell morphology using a microscope (Figure 3A). With RAD21 knockdown, the epithelial-like of MCF7 cells (represented as shCont) acquired fibroblast-like appearance (represented as shR#1) that correlated with EMT initiation. We also observed that the induction of VIM and β-catenin expression along with nuclear accumulation of β-catenin in RAD21KD cells compared to control cells (Figure 3B and 3C). Similar to epithelial- and mesenchymal- breast cancer cells shown in Figure 1C, reduction of E-cadherin levels and induction of VIM expression occurred with transition from an epithelial to mesenchymal morphology in RAD21-depleted epithelial breast cancer T47D cells. Consistent with the transition from an epithelial to mesenchymal morphology, the expression of other EMT-related molecules,

especially ones involved in the TGFB1-related signal pathway including TGFBR1 and TGFBR2 that are overexpressed in subpopulations with CSC features (CD44+) and metastatic tumors [46, 47], along with β-catenin was significantly induced in RAD21KD cells (Figure 3D). During EMT in cancer, cancer cells gradually acquire a migration ability to metastasize to other sites [48]. To evaluate cell motility in addition to morphological changes, we performed a wound-healing assay. Results showed that RAD21KD-MCF7 cells migrated more rapidly toward the wound sites compared to the control cells (Figure 3E). As mentioned above, it has been proposed that TGFB1 promotes and initiates EMT in cancer cells [40]. Additionally, another previous study showed that ITGA5 expression is induced through the TGFB1 intracellular Ca^{2+} signaling pathway in osteoblasts [49]. Contrary to this, other have demonstrated that ITGA5 activates TGFB signaling to initiate EMT [50-52]. Likewise, many studies have argued that TGFB1 and intergrins are associated and closely cross talk with each other in cells to modulate cellular metastasis [53, 54]. Given these data, we wondered if TGFB1 and ITGA5 expression induced by RAD21-depletion directly acts as a cue for starting the EMT process, or if the expression of one or both was simply a result of the acquisition of EMT properties via RAD21 depletion in epithelial cancer cells. We therefore knocked down either TGFB1 or ITGA5 in RAD21KD epithelial cancer cells with elevated TGFB1 and ITGA5 expression (Figure 3F and 3G). Transient knockdown of TGFB1 in RAD21KD-MCF7 cells with EMT traits showed that the levels of mesenchymal markers such as VIM, ZEB2, CDH2, and FN1, which were up-regulated in RAD21KD-MCF7 cells, were significantly reduced with ITGA5 down-regulation

(Figure 3F). The epithelial marker CDH1 was unaffected. Although a loss of E-cadherin expression is considered a critical marker of EMT plasticity, some studies showed that mere depletion of E-cadherin cannot fully promote EMT demonstrating that E-cadherin is not the sole pivotal molecule for EMT initiation [55, 56]. Similarly, ITGA5 depletion in RAD21KD-MCF7 cells notably reduced not only the expression of TGFB1 but also that of other EMT markers (Figure 3G), indicating that TGFB1 and ITGA5 expression promoted by RAD21KD individually and cooperatively affected the expression of each other as well as the EMT process in epithelial cancer cells. These findings suggested TGFB1 and ITGA5 are mutually regulated by each other rather than only ITGA5 regulated TGFB1 expression. Therefore, our results demonstrated that the induction of TGFB1 and ITGA5 expressions in depleted epithelial cancer cells directly promoted EMT and conferred mesenchymal-associated traits

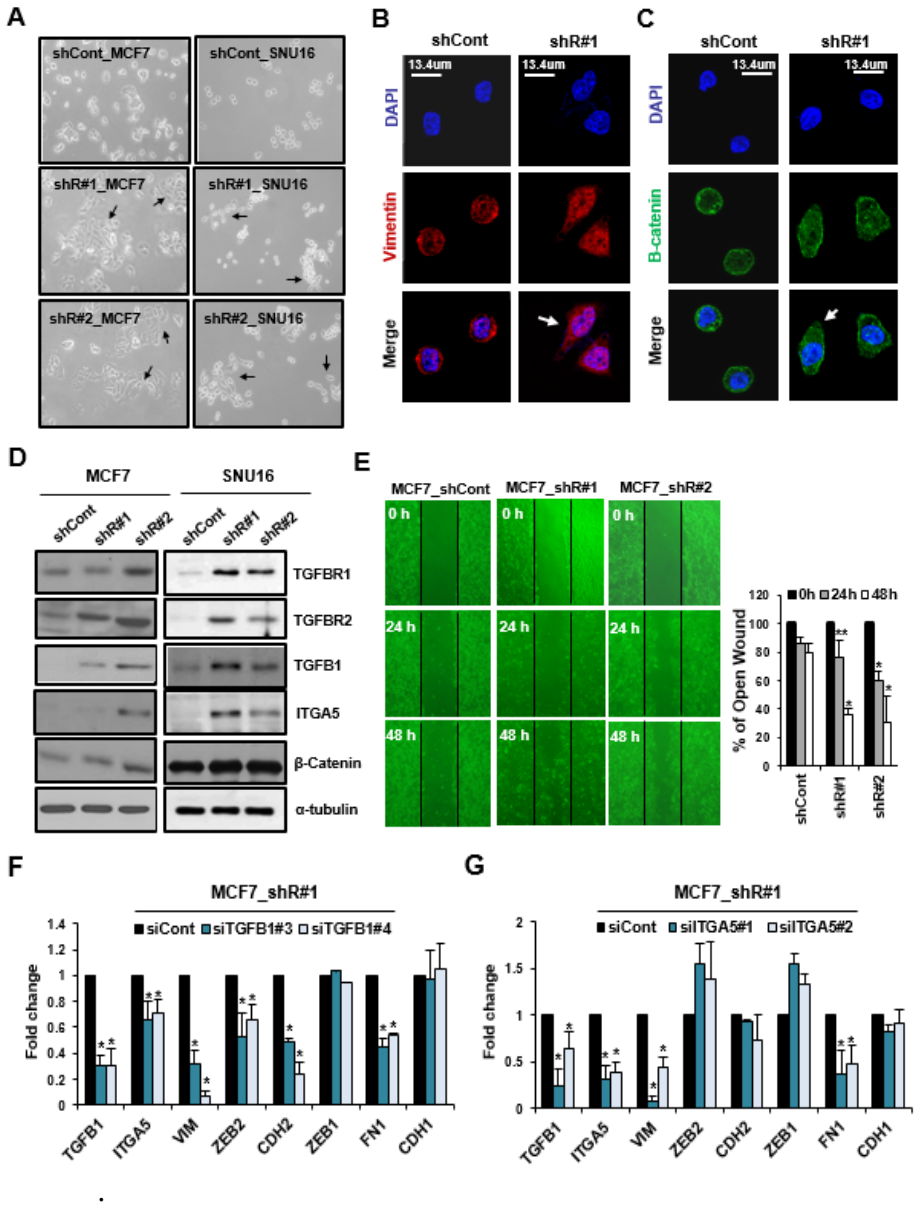

Figure 3. Disrupted RAD21 causes morphological changes from epithelial-like into fibroblast-like shapes.

(A) Imaging of RAD21KD-MCF7 and -SNU16 cells to assess cell morphology.

Depletion of RAD21 caused a conversion from an epithelial-like to fibroblast-like morphology (black arrowheads). Immunofluorescence staining for **(B)** VIM and **(C)** β-catenin in RAD21KD-SNU16 cells. The indicated cells were immunostained with antibody specific for VIM or β-catenin, and DAPI. **(D)** Western blots for EMT-markers TGFBR1, TGFBR2, TGFB1, ITGA5, and β-catenin in RAD21KD-MCF7 and -SNU16 cells. **(E)** Stable transfection of RAD21 shRNA in MCF7 cancer cells increased migration capabilities revealed by a wound-healing assay. Wound size was measured at 0, 24, and 48 h to calculate open wound rate (%). Data are presented as the mean ± s.d. for three independent experiments $*P < 0.01$ and; $**P < 0.05$. **(F)** qPCR was performed to measure the expression of EMT markers VIM, ZEB2, CDH2, ZEB1, and FN1 along with the epithelial marker CDH1 in shR#1_MCF7 cells after transfection with negative control, TGFB1 (siTGFB1#3 and siTGFB1#4), or **(G)** ITGA5 (siITGA5#1 and siITGA5#2) siRNAs for 48 h. Data are presented as the mean ± s.d. of three independent experiments $*P < 0.01$.

4. Gene-specific interchromosomal architecture in the *TGFB1* and *ITGA5* genes is dynamically regulated by cohesin.

We next ultimately wondered how RAD21KD significantly induced TGFB1 and ITGA5 expressions. To determine whether RAD21 was involved in chromatin organization, we evaluate physical interactions between RAD21 and the *TGFB1* or *ITGA5* gene. We also explored the relationship between the levels of RAD21 enrichment and gene transcription using a ChIP assay. First, we used mesenchymal breast cancer HCC1143 cells, which express low levels of both TGFB1 and ITGA5, and epithelial breast cancer MCF7 cells, in which TGFB1 and ITGA5 are highly expressed (Figure 2F), for the ChIP assay. RAD21 in the MCF7 cells was strongly enriched on the *TGFB1* promoter (indicated by amplicons 5, 6, and 7 of *TGFB1*) and the far-upstream region from the *ITGA5* gene promoter (indicated by amplicon 6 of *ITGA5*). In contrast, RAD21 weakly bound to the genes in mesenchymal HCC1143 cells, suggesting that the enrichment of RAD21 on the genes was inversely correlated with gene transcription levels. Additionally, we found that the strong binding of RAD21 to both the *TGFB1* and *ITGA5* genes was significantly reduced with RAD21KD in epithelial MCF7 and SNU16 cells (Figure 4A), implying the induction of *TGFB1* and *ITGA5* transcription was highly correlated with RAD21 enrichment on the gene. RAD21, one of the cohesin complex subunits, physically regulates the formation of the chromatin loop structure to control the gene-specific transcriptional environments [57]. We therefore speculated that RAD21 on the gene might modulate gene-specific chromatin architecture to regulate transcriptional activity of the gene.

A chromatin conformation capture (3C) assay for the *TGFB1* and *ITGA5* genes was thus performed [30] using RAD21KD-MCF7 or -SNU16 cells. Based on the ChIP data showing a high enrichment of RAD21 (Figure 4A), amplicon TGFB1_6 and amplicon ITGA5_6 were chosen as the anchors for the *TGFB1* and *ITGA5* genes, respectively, in RAD21KD-MCF7 or -SNU16 cells (Figure 4D and 4E). The results showed that strong binding of RAD21 formed gene-specific chromatin interactions within the *TGFB1* or *ITGA5* gene in shCont-MCF7 or -SNU16 cells (blue line, Figure 4D and 4E). Consistent with the loss of RAD21 binding on the genes due to RAD21KD (shown in Figure 4A), we also found that gene-specific chromatin interactions were disrupted by RAD21KD in both MCF7 and SNU16 cells (red line, Figure 4D and 4E). Similarly, another anchor (amplicon TGFB1_1 and amplicon ITGA5_1) also formed a chromatin loop structure that was disrupted on *TGFB1* and *ITGA5* gene by RAD21KD. Next, we determine why gene-specific chromatin architecture was related to gene transcription levels. A ChIP assay was performed to analyze two active transcription markers, RNA polymerase Ⅱ (Pol Ⅱ) and acetyl H3 (AcH3), using shCont- and RAD21KD-MCF7 or -SNU16 cells (Figure 4B and 4C). Expression of shControl in MCF7 or SNU16 cells led to low enrichment of Pol Ⅱ and AcH3 throughout the genes. On the other hand, RAD21KD significantly induced both factors to bind to the promoters of the genes. These findings suggested that the release of gene-specific chromatin architecture (shown in Figure 4D) might cause recruitment of these active transcriptional marks to the gene promoters to establish active transcriptional environments. Taken together, our results showed that the gene-specific chromatin architecture in *TGFB1* and *ITGA5* affected by RAD21 were

closely associated with transcriptional activities. High-chromatin interactions on the genes indicated low expression of the genes. In contrast, low-chromatin interaction on the genes signified high expression (Figure 4D and 4E).

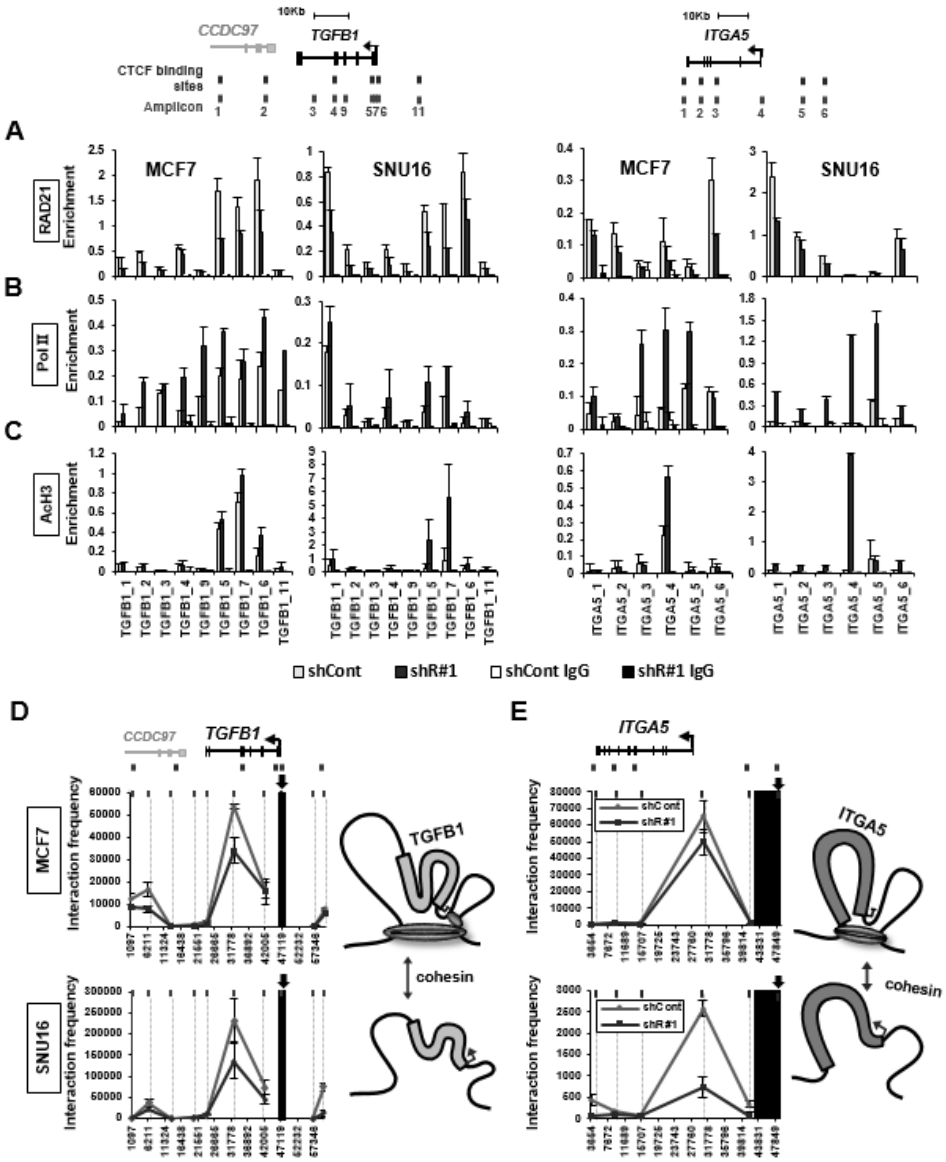

Figure 4. Released chromatin loop structure in TGFB1 and ITGA5 genes by RAD21KD leads to the recruitment of active transcription factors to the gene promoter.

TGFB1 and ITGA5 loci on chromosome 19q13.2 and chromosome 12q13.13, respectively. The location of putative CTCF binding sites and representative amplicon sites used for qPCR are shown with names below. A ChIP assay was performed for RAD21KD-MCF7 or -SNU16 cells using antibodies specific for **(A)** RAD21, **(B)** Pol II, **(C)** AcH3, or IgG (as a control). Enrichment was measured by qPCR and expressed relative to the total input (4%). Relative crosslinking frequencies among CTCF/RAD21 binding sites on the genes were measured with a 3C assay in the control GFP-shRNA (blue line) or RAD21KD (red line) -MCF7 or -SNU16 cells on day 30 after lentiviral transduction. **(D)** BamH1 or **(E)** Xba I restriction sites on the *TGFB1* or *ITGA5* gene, respectively, appear as gray shaded bars. Black shading indicates the anchor fragment. Each value was normalized to crosslinking frequency at the *ERCC3* gene. The maximum crosslinking frequency was set at 1. (Mean ± SEM, n = 3).

5. Cancer stem-like breast cancer cells show a released higher-order chromatin structure of *TGFB1*- and *ITGA5*-mediated by RAD21, which correlated to the high transcriptional expressions and mesenchymal properties

Since it has been reported that the most types of tumor overexpress Rad21 [58-60], we speculated that only small population of tumor burdens with a low expression of Rad21 might be responsible for the cancer metastasis to the second metastatic site. To verify this, we analyzed transcript expression data obtained from The Cancer Genome Atlas (TCGA). A total of 80 breast tumor tissues and matched normal samples, including all subtypes, were analyzed to measure the transcript levels of RAD21, CDH1, VIM, TGFB1, ITGA5, ZEB1/2, and SNAI1/2. The results revealed that the RAD21 mRNA levels in the tumor samples were higher than those in normal cells although we could not assess the protein expression levels. And the tumor samples showed obvious epithelial traits, consistent with our data showing the relationship between RAD21 expression and the EMT.

In contradiction of our hypothesis, relatively high levels of TGFB1 mRNA expression were observed in the tumor samples compared to normal samples. Even though it is known that TGFB has multiple functions, it primarily acts as a tumor suppressor via anti-proliferative activity in normal cells. Furthermore, this factor contributes to the differentiation, proliferation, and migration of aggressive tumor cells [61, 62]. We therefore suggested that the high levels of TGFB1 expression in tumors with high RAD21 expression, independent from transcriptional up-regulation caused by reduced RAD21 involved in tumor metastasis, might be due to a

proliferative effect of TGFB1 on tumor cells. This was supported by an absence of significant changes in ITGA5 mRNA levels when comparing normal and tumor samples ($P = 0.7468$). Since primary tumors are composed of heterogeneous tumor cells, there might be certain cells with initial migratory properties. However, we could not readily detect this type of population due to their small portion like cancer stem cells (CSCs).

To understand this, we ultimately expanded our model to include CSCs since EMT has been known to be highly linked to CSC [23, 47, 63]. While traditional models of tumor initiation suggest that cancer cells arise from environmental factors or genetic alterations and then gradually acquire aggressive properties, the CSC hypothesis argues that cancer development is attributed to CSCs which consist of a small population of heterogeneous tumors that can be responsible for tumor proliferation and initiation [64]. The most important feature of CSCs has been reported to be the possession EMT features that allow cell dissemination, invasion, and migration.

We therefore used MDA-MB-453 breast cancer cell derived cancer stem-like cells (CSLCs) [25, 26] positive for CD44/CD133/CD147 expression, which are well known markers of CSCs. Consistent with previous studies [23, 25, 65], high levels of mesenchymal-related genes including ZEB2, FN1, TWIST, VIM, TGFBR1, TGFBR2, and β-catenin were observed in the CSLCs, indicating that these cells had significant mesenchymal properties (Figure 5A and 5B). However, we unexpectedly discovered high levels of E-cadherin in the CSLCs (Figure 5A and 5B), suggesting

that it can serve as an evidence of that sole E-cadherin alone is not sufficient for EMT initiation and the CSCs have partial EMT properties.

Next, we checked and compared the levels of RAD21 expression between MDM-MB-453 CSLCs and the parental cells. As shown in Figure 5A and 5B, we observed that the expression of both RAD21 mRNA and protein in the CSLCs was reduced to less than 1.5-fold compared to levels found in the parental cells. Although the mRNA levels of RAD21 per se were lower in the CSLCs compared to the parental cells, which was unlike the patterns of mRNA expressions found in mesenchymal and epithelial breast cancer cell lines (Figure 1C), the mRNA in the CSLCs was relatively unstable compared to that in the parental cells. These findings were consistent with results presented in Figure 1D. In addition to a low level of RAD21 expression, we also observed high expression of TGFB1 and ITGA5 mRNA in the CSLCs, corresponding to results for the RAD21KD cells. To determine if high levels of TGFB1 and ITGA5 expression found in the CSLCs formed its chromatin architecture like in RAD21KD epithelial cells (shown in Figure 4D and 4E), we performed a 3C assay using the CSLCs and parental cells (Figure 5C). In CSLCs with high expression of TGFB1 and ITGA5, lower interaction frequencies were observed within both the *TGFB1* and *ITGA5* genes compared to those in the parental cells. To determine if the gene-specific chromatin architectures were directly mediated by RAD21 and regulated gene transcription, we assessed the enrichment of RAD21, AcH3, and Pol Ⅱ on the genes using a ChIP assay (Figure 5D). Consistent with the 3C data, RAD21 binding on the genes was overly lower in the CSLCs

compared to the parental cells. Conversely, the markers corresponding to transcriptional activity, AcH3 and Pol Ⅱ, were notably enriched on the promoter of the genes, consistent with gene transcription levels, indicating that the CSLCs might also be regulated and maintained by TGFB1 and ITGA5 gene-specific chromatin interactions. Chromatin loop open structure in each gene easily recruit transcription factors to the gene promoter to activate gene transcriptions like RAD21KD epithelial cancer cells. Collectively, these results strongly support our hypothesis that cohesin-mediated three dimensional chromatin structures are responsible for regulating and maintaining EMT plasticity in a small population of tumors or cancer stem cell model by controlling transcriptional activities of EMT-related genes associated with metastasis, thereby conferring migratory and invasive properties.

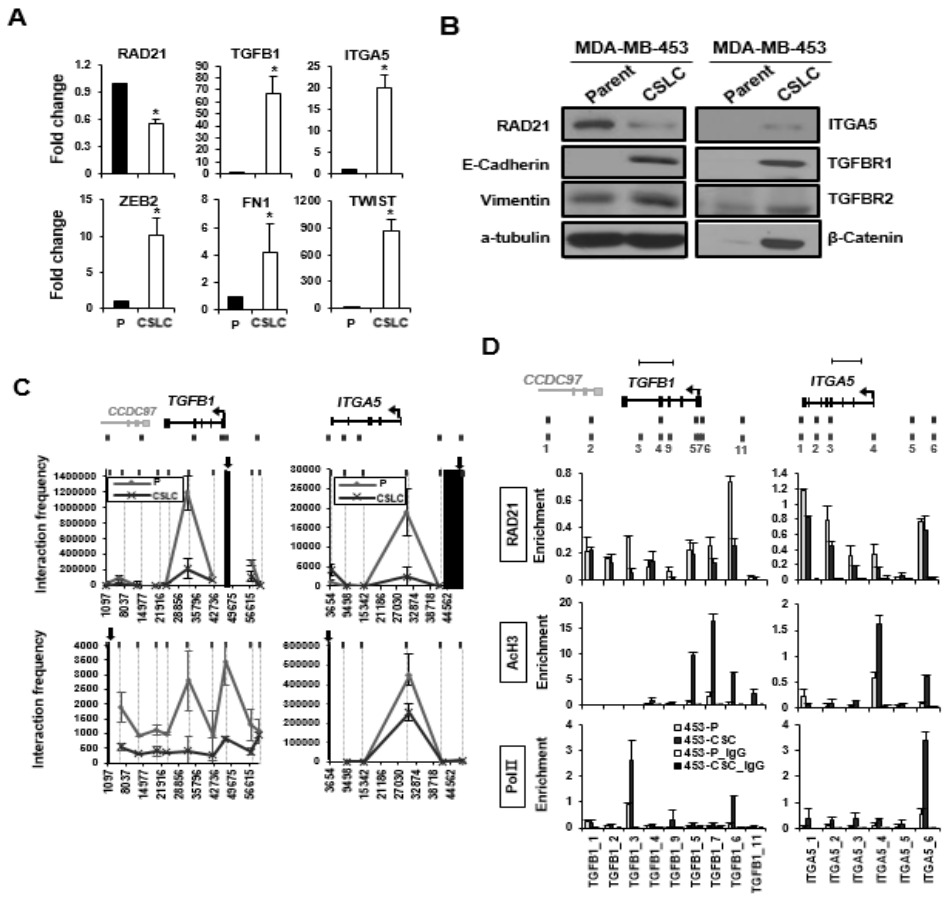

Figure 5. RAD21 is responsible for metastatic characteristics in CSLCs.

(A-B) Parent MDA-MB-453 breast cancer cells (P) and the corresponding CSLCs sorted according to the CD44+ cancer stem cell marker showed that the close RAD21 expression. *TGFB1* and *ITGA5* loci on chromosome 19q13.2 and chromosome 12q13.13, respectively. Location of putative CTCF binding sites and representative amplicon sites used for qPCR are shown with names below. **(C)** Relative crosslinking frequencies among CTCF/RAD21 binding sites on the genes were

measured with a 3C assay in the control GFP-shRNA (blue line) or RAD21-KD (red line)-MCF7 or -SNU16 cells on day 30 after lentiviral transduction. BamH1 or Xba I restriction sites on the *TGFB1* or *ITGA5* gene, respectively, appear as gray shaded bars. Black shading indicates the anchor fragment. Each value was normalized to the crosslinking frequency at the *ERCC3* gene. **(D)** A ChIP assay was performed for the CSLCs (red bar) or parental cells (blue bar) using antibodies specific for RAD21, AcH3, Pol II, or IgG (as the control). Enrichment was measured by qPCR and reported relative to the total input (4%).

6. Overexpression of RAD21 in mesenchymal breast cancer cells reduces TGFB1 and ITGA5 expression, concomitant with enhancement of intra-chromosomal interaction on the gene.

To confirm the function of RAD21 on the transcriptional regulation of TGFB1 and ITGA5 through modulating the transcriptionally repressive gene-specific chromatin architecture in epithelial cancer cells, we overexpressed RAD21 in MDA-MB-231 mesenchymal breast cancer cell and MDA-MB-453 CSLC cell with a low level of RAD21 expression (Figures 6A-D). Although the transient overexpression of RAD21 did not appear to be sufficient in MDA-MB-231 and

CSLC cells, we clearly found that the overexpressed RAD21 in mesenchymal cancer cells reduced TGFB1 and ITGA5 gene transcriptions (Figures 6A-B). Furthermore, most of the EMT markers that were induced in the RAD21KD-epithelial cells, such as VIM, ZEB1, and SNAI2, were decreased following RAD21 overexpression. These gene expression changes induced by RAD21 overexpression also led to the induction of a direct RAD21 molecule binding and the decreased Pol II and H3K9ac on the *TGFB1* and *ITGA5* gene (Figure 6C). Using a 3C assay, we determined that the induction of RAD21 binding on each *TGFB1* and *ITGA5* gene enhanced the intra-chromosomal interaction in each genes.

Taken together, these results suggest that TGFB1 and ITGA5 gene transcription in cancer cells might depend on its three-dimensional chromatin structure-mediated by cohesin complex, playing a crucial role in the epithelial to mesenchymal transition and mesenchymal to epithelial transition.

During tumorigenesis, individual tumor cells responsible for metastasis might accurately regulate the transcriptional activity of upstream EMT-related genes such as *TGFB1* and *ITGA5*, which are thought to be responsible for EMT initiation, through dynamic changes in higher-order chromatin loop structures mediated by the cohesin complex (Figure 6E).

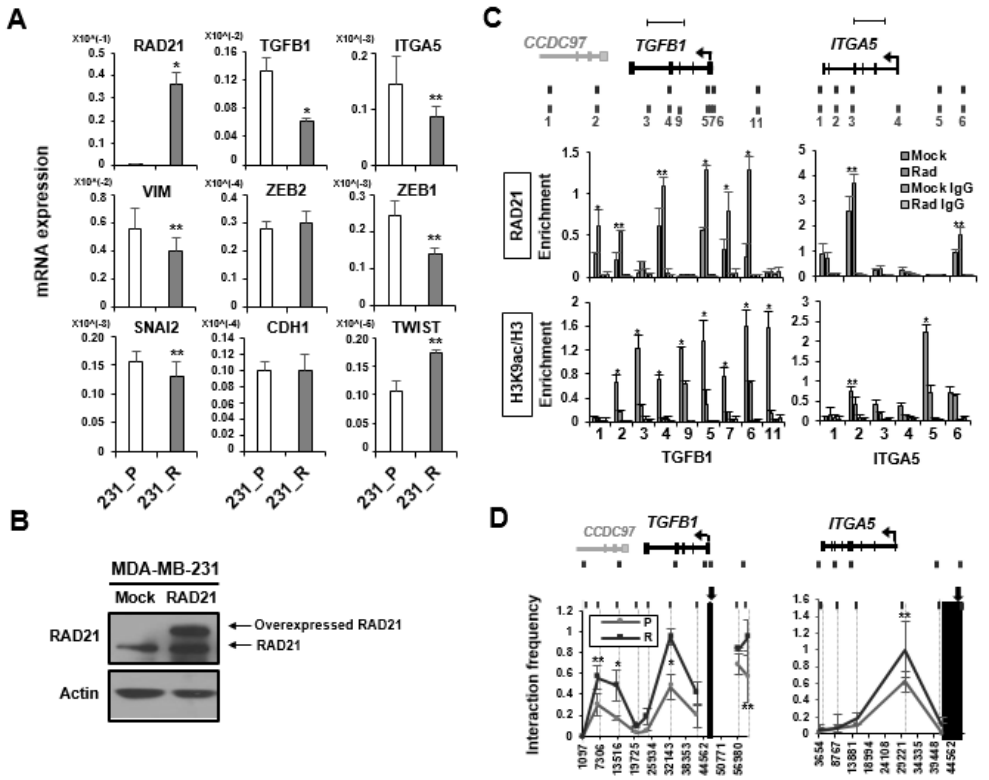

Figure 6. RAD21 overexpression in MDA-MB-231 mesenchymal cancer cells decreases TGFB1 and ITGA5 expression with enhanced intra-chromosomal interactions.

(A) The relative mRNA expression levels of EMT-related genes in RAD21-overexpressing MDA-MB-231 cells were quantified and normalized by 18s transcript. Empty vector-expressing MDA-MB-231 control cells are indicated by 231_P; RAD21-expressing MDA-MB-231 cells are indicated by 231_R. The data shown are the mean ± S.D. for three independent experiments. *$P < 0.01$, **$P < 0.05$. Statistical significance was validated by Student's *t*-tests. **(B)** Western blots for

RAD21 in RAD21-overexpressing MDA-MB-231 cells. **(C)** A ChIP assay was performed for RAD21-overexpressing MDA-MB-231 and the empty vector expressing cells using antibodies specific for RAD21, Pol II, and H3K9ac, or IgG (as a control). Enrichment was measured by qPCR and expressed relative to the total input (4%). ChIP signals for H3K9ac were normalized to total H3. Results for at least three chromatin preparations are shown ± S.E.M. *$P < 0.01$, **$P < 0.05$. Statistical significance was validated by Student's *t*-tests. **(D)** Relative crosslinking frequencies among CTCF/RAD21 binding sites on the genes were measured with a 3C assay in the control (blue line) or RAD21-overexpressing (red line) MDA-MB-231 cells on day 10 after lentiviral transduction. BamH1 or XbaI restriction sites on the *TGFB1* or *ITGA5* gene, respectively, appear as gray shaded bars. Black shading indicates the anchor fragment. Each value was normalized to crosslinking frequency at the *ERCC3* gene. The maximum crosslinking frequency was set at 1. (means ± S.E.M, n = 3). *$P < 0.01$, **$P < 0.05$. Statistical significance was validated by Student's *t*-tests.

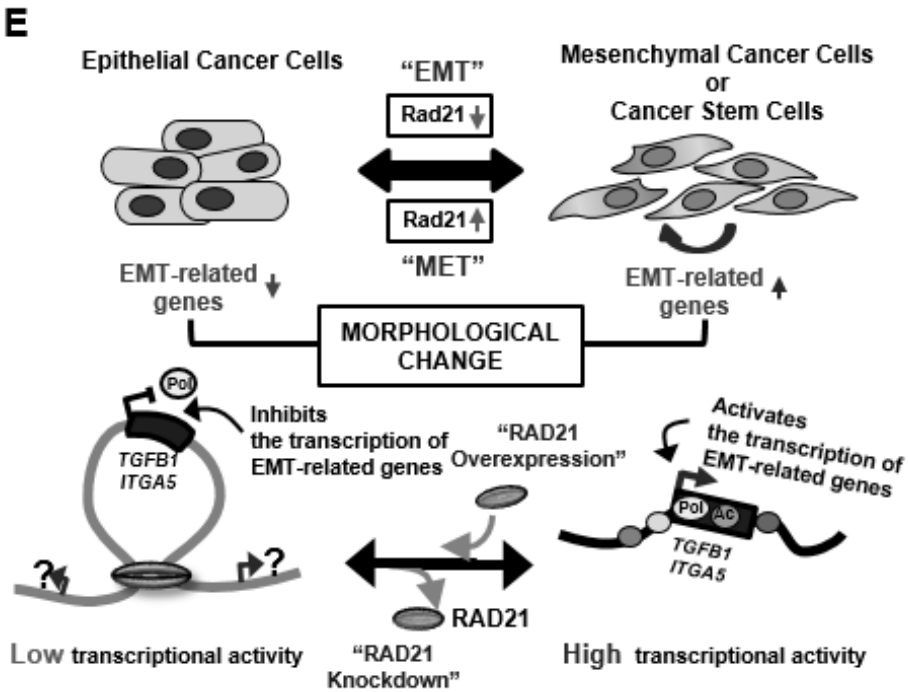

Figure 6. (E) A proposed model of cohesin-mediated dynamic chromatin architecture of the TGFB1 and ITGA5 genes associated with EMT plasticity. Tumor cells that have undergone EMT are characterized by proposed chromatin architectures. In epithelial cancer cells, cohesin tightly mediates distant intrachromosomal interactions in the TGFB1 and ITGA5 genes. When RAD21 mRNA stability is lost, RAD21 bound on the genes is reduced and intrachromosomal interactions in the genes are released, causing active recruitment of the transcriptional complex to the gene promoters. This enhances gene transcription and the cells acquire mesenchymal properties such as enhanced mobility and morphological changes.

DISCUSSION

In the current study, we addressed the role of the cohesin complex in the dynamic transition of epithelial to mesenchymal cancer cells by altering distant chromatin interactions of *TGFB1* and *ITGA5* genes and inducing their transcriptional activities. These two factors are considered upstream molecules that influence the EMT in epithelial cancer cells and CSCs.

We analyzed transcript expression data for primary breast tumor and normal tissue samples from the TCGA database. Interestingly, higher expression of RAD21 was observed in the tumor tissues compared to the normal samples. Since primary or metastatic tumor samples obtained by biopsy are already differentiated and sufficiently have lost mesenchymal properties that proceed MET process [4, 66], the tumor samples might have a high level of RAD21 expression similar to epithelial cancer cell lines. This suggests that only small proportion of tumors or CSCs might play an important role in metastasis.

Differences in RAD21 expression between cells with epithelial or mesenchymal traits were due to variations in mRNA stability. However, we could not determine how the stability of RAD21 mRNA is regulated or the stage of tumorigenesis and mechanisms associated with the loss of mRNA stability. Further study is therefore required to understand the underlying mechanisms that govern dynamic RAD21 during tumorigenesis. We can, however, propose that chromatin dynamics mediated by the higher-order chromatin structural molecule cohesin might actively confer epithelial or mesenchymal properties depending on the surrounding

environment or cell fate. Interestingly, we observed a significant induction of TGFB1 and ITGA5 expression immediately following RAD21 knockdown in MCF7 and SNU16 cells. TGF-β has been known as a potent inducer of the EMT in mammary cells and increases stem-like properties in human breast cancer cells [47, 67]. ITGA5 is expressed during tumor development and has been implicated in EMT induction. This may explain why highly invasive cancer cells have higher levels of ITGA5 and overexpression of this factor increases the metastatic capacity [68, 69]. Based on the data shown in Figure 3F and 3G, we postulated that either TGFB1 or ITGA5 expression induced by RAD21 depletion might directly result in the induction of mesenchymal-related genes, most of which are well known repressors of CDH1, but not the epithelial-related gene CDH1 itself. Up-regulation of these genes clearly led to a morphological transition from epithelial to mesenchymal phenotypes and provided the cells with motility and invasive capabilities (Figure 3). Intriguingly, we observed a relatively high level of E-cadherin in MDA-MB-453-derived CSLCs compared to the parental cells (Figure 5C). As previously mentioned, this finding suggested that either E-cadherin may be not the sole molecule responsible for EMT initiation without orchestrate regulations or changes in other EMT-related factors or MDA-MB-453 derived CSLCs may not be completely transformed into mesenchymal and invasive cells. One more thing we suggest that changes in mesenchymal-related gene expressions are more susceptible to alterations in the expression of upstream factors for EMT initiation (like TGFB1 and ITGA5) than epithelial-related genes.

We demonstrated that the expression of TGFB1 and ITGA5 closely relies on the

gene-specific three dimensional chromatin structure mediated by cohesin (Figure 4). Unsurprisingly, enrichment of RAD21 on the genes affected the formation of gene-specific chromatin loop structures. While strong binding of RAD21 on the gene forms strong chromatin interactions within the genes, low enrichment of RAD21 leads to a loss of the interactions. Interestingly, gene-specific chromatin interactions in CSLCs were very weak compared to those in the parental cells despite the persistent RAD21 expression in the CSCLs (Figure 5D). This significant difference in the chromatin interaction for TGFB1 and ITGA5 between CSLCs and the parental cells largely affected expression of the genes, suggesting that transcriptions related with EMTgene may be dependent on chromatin interactions.

Depending on where the chromatin interactions are formed, chromatin loop structures are categorized into five distinct patterns with transcriptional activity (PolⅡ) and several histone modification signatures [70]. Of the categories, one features chromatin signatures of active characteristics with enrichment of PolⅡ, H3K4me1, H3K36me3 or AcH3, and depleted repressive marks such as H3K9, H3K27 methylation inside the loops. Conversely, another pattern features chromatin loops with extensive methylation of H3K9 and H3K27 but loss of active marks with in. As shown in Figure 4, gene-specific chromatin interactions between gene promoter and intragenic (*TGFB1*) or upstream region (*ITGA5*) in epithelial cancer cells seem to inhibit or disturb the recruitment of transcriptional factors like PolⅡ and AcH3, thereby preventing transcription. Consistent with the transcription levels

shown in Figure 4, transcriptional activities inside the loops were significantly reduced when gene-specific chromatin interactions are released by insufficient RAD21 for chromatin interaction in epithelial cancer cells like MCF7 and SNU16. In addition to epithelial breast and gastric cancer cell lines, weak binding of PolⅡ and AcH3 to the gene promoters that disrupted chromatin interactions was observed in CSLCs with low RAD21 expression compared to the parental cells (Figure 5E). Intriguingly, strong binding of PolⅡ on 3' end of TGFB1 was observed in MDA-MB-453-derived CSLCs unlike MCF7 and SNU16 cells (Figure 5D comparing to Figure 4B). We postulate that there might be unknown non-coding RNA or cis-regulatory sequences only in this cell [71].

Finally, we used primary tumor data and cancer stem-like cells to clarify the clinical implications of our study findings. As described above, we obtained results showing that the complete primary tumor samples had epithelial properties rather than mesenchymal traits. We suggested that the MET had already occurred in most of the population. Due to difficulties with isolating and detecting very small populations possessing mesenchymal traits or CSCs from tumors [1, 7], we obtained CSLCs derived from the breast cancer MDA-MB-453 cell line [25, 26]. Using the CSLC model, we were able to obtain the same results acquired with breast cancer cell lines with mesenchymal properties (MDA-MB-231, HCC1143, and MDA-MB-157) and RAD21 depleted epithelial cancer cells (RAD21KD-MCF7, -T47D, -SNU16, and -SNU620 cells).

Given our results and the fact that the recent studies showed that CSCs were re-

generated from non-CSCs by the induction of EMT systems [23, 72], we speculated that the CSCs might use the same biological mechanisms as EMT properties to metastasize or migrate that are regulated by the dynamic changes in cohesin-mediated chromatin interaction of EMT-related genes, although these have been known not to be genetically and epigenetically identical.

The present study supports the theory that a specific subpopulation of cancer cells is responsible for tumor metastasis, similar to the cancer stem cell hypothesis. An important point we can suggest based on our study in this regard is that inhibiting overexpression of the cohesin complex in most aggressive tumors should be carefully considered to avoid metastasis caused by released three-dimensional chromatin loop structures in the *TGFB1* and *ITGA5* gene due to insufficient cohesin complexes

REFERENCES

Ⅰ. REDUCED COHESIN DESTABILIZES HIGH-LEVEL GENE AMPLIFICATION BY DISRUPTING PRE-REPLICATION COMPLEX BINDINGS IN HUMAN CANCERS WITH CHROMOSOMAL INSTABILITY

1. Surani, M.A., K. Hayashi, and P. Hajkova, *Genetic and epigenetic regulators of pluripotency.* Cell, 2007. **128**(4): p. 747-62.
2. Lengauer, C., K.W. Kinzler, and B. Vogelstein, *Genetic instabilities in human cancers.* Nature, 1998. **396**(6712): p. 643-9.
3. Negrini, S., V.G. Gorgoulis, and T.D. Halazonetis, *Genomic instability--an evolving hallmark of cancer.* Nat Rev Mol Cell Biol, 2010. **11**(3): p. 220-8.
4. Albertson, D.G., *Gene amplification in cancer.* Trends Genet, 2006. **22**(8): p. 447-55.
5. Santarius, T., et al., *A census of amplified and overexpressed human cancer genes.* Nat Rev Cancer, 2010. **10**(1): p. 59-64.
6. Tanaka, H. and M.C. Yao, *Palindromic gene amplification--an evolutionarily conserved role for DNA inverted repeats in the genome.* Nat Rev Cancer, 2009. **9**(3): p. 216-24.
7. Shimizu, N., *Extrachromosomal double minutes and chromosomal homogeneously staining regions as probes for chromosome research.* Cytogenet Genome Res, 2009. **124**(3-4): p. 312-26.
8. Hastings, P.J., et al., *Mechanisms of change in gene copy number.* Nat Rev Genet, 2009. **10**(8): p. 551-64.
9. Kondratova, A., et al., *Replication fork integrity and intra-S phase checkpoint suppress gene amplification.* Nucleic Acids Res, 2015. **43**(5): p. 2678-90.
10. Coquelle, A., et al., *Expression of fragile sites triggers intrachromosomal mammalian gene amplification and sets boundaries to early amplicons.* Cell, 1997. **89**(2): p. 215-25.
11. Stuart, D. and W.R. Sellers, *Linking somatic genetic alterations in cancer to therapeutics.* Curr Opin Cell Biol, 2009. **21**(2): p. 304-10.
12. Dorsett, D. and L. Strom, *The ancient and evolving roles of cohesin in gene expression and DNA repair.* Curr Biol, 2012. **22**(7): p. R240-50.
13. Nasmyth, K. and C.H. Haering, *Cohesin: its roles and mechanisms.* Annu Rev Genet, 2009. **43**: p. 525-58.
14. Watrin, E. and J.M. Peters, *The cohesin complex is required for the DNA damage-induced G2/M checkpoint in mammalian cells.* EMBO J, 2009. **28**(17): p. 2625-35.
15. Barber, T.D., et al., *Chromatid cohesion defects may underlie chromosome instability in human colorectal cancers.* Proc Natl Acad Sci U S A, 2008. **105**(9): p.

3443-8.
16. Solomon, D.A., et al., *Mutational inactivation of STAG2 causes aneuploidy in human cancer.* Science, 2011. **333**(6045): p. 1039-43.
17. Hou, C., R. Dale, and A. Dean, *Cell type specificity of chromatin organization mediated by CTCF and cohesin.* Proc Natl Acad Sci U S A, 2010. **107**(8): p. 3651-6.
18. Nativio, R., et al., *Cohesin is required for higher-order chromatin conformation at the imprinted IGF2-H19 locus.* PLoS Genet, 2009. **5**(11): p. e1000739.
19. Hadjur, S., et al., *Cohesins form chromosomal cis-interactions at the developmentally regulated IFNG locus.* Nature, 2009. **460**(7253): p. 410-3.
20. Gosalia, N., et al., *Architectural proteins CTCF and cohesin have distinct roles in modulating the higher order structure and expression of the CFTR locus.* Nucleic Acids Res, 2014. **42**(15): p. 9612-22.
21. Losada, A., *Cohesin in cancer: chromosome segregation and beyond.* Nat Rev Cancer, 2014. **14**(6): p. 389-93.
22. Yun, W.J., et al., *The hematopoietic regulator TAL1 is required for chromatin looping between the beta-globin LCR and human gamma-globin genes to activate transcription.* Nucleic Acids Res, 2014. **42**(7): p. 4283-93.
23. Rhodes, J.M., M. McEwan, and J.A. Horsfield, *Gene regulation by cohesin in cancer: is the ring an unexpected party to proliferation?* Mol Cancer Res, 2011. **9**(12): p. 1587-607.
24. Deb, S., et al., *RAD21 cohesin overexpression is a prognostic and predictive marker exacerbating poor prognosis in KRAS mutant colorectal carcinomas.* Br J Cancer, 2014. **110**(6): p. 1606-13.
25. Yadav, S., et al., *Role of SMC1 in overcoming drug resistance in triple negative breast cancer.* PLoS One, 2013. **8**(5): p. e64338.
26. Morales, C., et al., *Genetic determinants of methotrexate responsiveness and resistance in colon cancer cells.* Oncogene, 2005. **24**(45): p. 6842-7.
27. Park, J.G., et al., *Characteristics of cell lines established from human gastric carcinoma.* Cancer Res, 1990. **50**(9): p. 2773-80.
28. Gravalos, C. and A. Jimeno, *HER2 in gastric cancer: a new prognostic factor and a novel therapeutic target.* Ann Oncol, 2008. **19**(9): p. 1523-9.
29. Ku, J.L. and J.G. Park, *Biology of SNU cell lines.* Cancer Res Treat, 2005. **37**(1): p. 1-19.
30. Song, S.H., C. Hou, and A. Dean, *A positive role for NLI/Ldb1 in long-range beta-globin locus control region function.* Mol Cell, 2007. **28**(5): p. 810-22.
31. Yun, J., et al., *Gene silencing of EREG mediated by DNA methylation and histone modification in human gastric cancers.* Lab Invest, 2012. **92**(7): p. 1033-44.
32. Song, S.H., et al., *Multiple functions of Ldb1 required for beta-globin activation during erythroid differentiation.* Blood, 2010. **116**(13): p. 2356-64.
33. Garnis, C., T.P. Buys, and W.L. Lam, *Genetic alteration and gene expression modulation during cancer progression.* Mol Cancer, 2004. **3**: p. 9.
34. Kim, J.I., et al., *A highly annotated whole-genome sequence of a Korean individual.*

Nature, 2009. **460**(7258): p. 1011-5.
35. Olshen, A.B., et al., *Circular binary segmentation for the analysis of array-based DNA copy number data.* Biostatistics, 2004. **5**(4): p. 557-72.
36. Trapnell, C., et al., *Transcript assembly and quantification by RNA-Seq reveals unannotated transcripts and isoform switching during cell differentiation.* Nat Biotechnol, 2010. **28**(5): p. 511-5.
37. Wang, L., et al., *DEGseq: an R package for identifying differentially expressed genes from RNA-seq data.* Bioinformatics, 2010. **26**(1): p. 136-8.
38. Mefford, H.C., et al., *Recurrent rearrangements of chromosome 1q21.1 and variable pediatric phenotypes.* N Engl J Med, 2008. **359**(16): p. 1685-99.
39. Guillou, E., et al., *Cohesin organizes chromatin loops at DNA replication factories.* Genes Dev, 2010. **24**(24): p. 2812-22.
40. Dekker, J., et al., *Capturing chromosome conformation.* Science, 2002. **295**(5558): p. 1306-11.
41. Tolhuis, B., et al., *Looping and interaction between hypersensitive sites in the active beta-globin locus.* Mol Cell, 2002. **10**(6): p. 1453-65.
42. Spilianakis, C.G., et al., *Interchromosomal associations between alternatively expressed loci.* Nature, 2005. **435**(7042): p. 637-45.
43. Hagege, H., et al., *Quantitative analysis of chromosome conformation capture assays (3C-qPCR).* Nat Protoc, 2007. **2**(7): p. 1722-33.
44. Parelho, V., et al., *Cohesins functionally associate with CTCF on mammalian chromosome arms.* Cell, 2008. **132**(3): p. 422-33.
45. Martin, M.M., et al., *Genome-wide depletion of replication initiation events in highly transcribed regions.* Genome Research, 2011. **21**(11): p. 1822-1832.
46. Abbas, T., M.A. Keaton, and A. Dutta, *Genomic instability in cancer.* Cold Spring Harb Perspect Biol, 2013. **5**(3): p. a012914.
47. Siddiqui, K., K.F. On, and J.F. Diffley, *Regulating DNA replication in eukarya.* Cold Spring Harb Perspect Biol, 2013. **5**(9).
48. Alabert, C. and A. Groth, *Chromatin replication and epigenome maintenance.* Nat Rev Mol Cell Biol, 2012. **13**(3): p. 153-67.
49. Okada, N. and N. Shimizu, *Dissection of the beta-globin replication-initiation region reveals specific requirements for replicator elements during gene amplification.* PLoS One, 2013. **8**(10): p. e77350.
50. Harada, S., N. Sekiguchi, and N. Shimizu, *Amplification of a plasmid bearing a mammalian replication initiation region in chromosomal and extrachromosomal contexts.* Nucleic Acids Res, 2011. **39**(3): p. 958-69.
51. O'Neil, N.J., D.M. van Pel, and P. Hieter, *Synthetic lethality and cancer: cohesin and PARP at the replication fork.* Trends Genet, 2013.
52. Terret, M.E., et al., *Cohesin acetylation speeds the replication fork.* Nature, 2009. **462**(7270): p. 231-4.
53. MacAlpine, H.K., et al., *Drosophila ORC localizes to open chromatin and marks sites of cohesin complex loading.* Genome Res, 2010. **20**(2): p. 201-11.
54. Courbet, S., et al., *Replication fork movement sets chromatin loop size and origin*

choice in mammalian cells. Nature, 2008. **455**(7212): p. 557-60.
55. Hashimoto, Y., F. Puddu, and V. Costanzo, *RAD51- and MRE11-dependent reassembly of uncoupled CMG helicase complex at collapsed replication forks.* Nat Struct Mol Biol, 2012. **19**(1): p. 17-24.
56. Costa, A., et al., *The structural basis for MCM2-7 helicase activation by GINS and Cdc45.* Nat Struct Mol Biol, 2011. **18**(4): p. 471-7.
57. Chen, X., G. Liu, and M. Leffak, *Activation of a human chromosomal replication origin by protein tethering.* Nucleic Acids Res, 2013. **41**(13): p. 6460-74.
58. Waga, S. and B. Stillman, *The DNA replication fork in eukaryotic cells.* Annu Rev Biochem, 1998. **67**: p. 721-51.
59. Mechali, M., *Eukaryotic DNA replication origins: many choices for appropriate answers.* Nat Rev Mol Cell Biol, 2010. **11**(10): p. 728-38.
60. Moyer, S.E., P.W. Lewis, and M.R. Botchan, *Isolation of the Cdc45/Mcm2-7/GINS (CMG) complex, a candidate for the eukaryotic DNA replication fork helicase.* Proc Natl Acad Sci U S A, 2006. **103**(27): p. 10236-41.
61. Mannini, L., S. Menga, and A. Musio, *The expanding universe of cohesin functions: a new genome stability caretaker involved in human disease and cancer.* Hum Mutat, 2010. **31**(6): p. 623-30.
62. Kon, A., et al., *Recurrent mutations in multiple components of the cohesin complex in myeloid neoplasms.* Nat Genet, 2013. **45**(10): p. 1232-7.
63. Deardorff, M.A., et al., *RAD21 mutations cause a human cohesinopathy.* Am J Hum Genet, 2012. **90**(6): p. 1014-27.
64. Ottini, L., et al., *Patterns of genomic instability in gastric cancer: clinical implications and perspectives.* Ann Oncol, 2006. **17 Suppl 7**: p. vii97-102.
65. Schaaf, C.A., et al., *Genome-wide control of RNA polymerase II activity by cohesin.* PLoS Genet, 2013. **9**(3): p. e1003382.
66. Nitzsche, A., et al., *RAD21 cooperates with pluripotency transcription factors in the maintenance of embryonic stem cell identity.* PLoS One, 2011. **6**(5): p. e19470.
67. Coquelle, A., et al., *Induction of multiple double-strand breaks within an hsr by meganucleaseI-SceI expression or fragile site activation leads to formation of double minutes and other chromosomal rearrangements.* Oncogene, 2002. **21**(50): p. 7671-9.
68. Negi, L.M., et al., *Role of CD44 in tumour progression and strategies for targeting.* J Drug Target, 2012. **20**(7): p. 561-73.
69. Meyer, N. and L.Z. Penn, *Reflecting on 25 years with MYC.* Nat Rev Cancer, 2008. **8**(12): p. 976-90.
70. Katoh, M. and M. Katoh, *Recombination cluster around FGFR2-WDR11-HTPAPL locus on human chromosome 10q26.* Int J Mol Med, 2003. **11**(5): p. 579-83.

Ⅱ. DISRUPTION OF INTRACHROMOSOMAL INTERACTIONS BY DEFICIENT COHESIN INITIATE EPITHELIAL-MESENCHYMAL TRANSITION AND STEMNESS IN CANCER

1. Chaffer, C.L. and R.A. Weinberg, *A perspective on cancer cell metastasis.* Science, 2011. **331**(6024): p. 1559-64.
2. Gunasinghe, N.P., et al., *Mesenchymal-epithelial transition (MET) as a mechanism for metastatic colonisation in breast cancer.* Cancer Metastasis Rev, 2012. **31**(3-4): p. 469-78.
3. Nguyen, D.X. and J. Massague, *Genetic determinants of cancer metastasis.* Nat Rev Genet, 2007. **8**(5): p. 341-52.
4. Kalluri, R. and R.A. Weinberg, *The basics of epithelial-mesenchymal transition.* J Clin Invest, 2009. **119**(6): p. 1420-8.
5. Yokota, J., *Tumor progression and metastasis.* Carcinogenesis, 2000. **21**(3): p. 497-503.
6. Nieto, M.A., *The ins and outs of the epithelial to mesenchymal transition in health and disease.* Annu Rev Cell Dev Biol, 2011. **27**: p. 347-76.
7. Medema, J.P., *Cancer stem cells: the challenges ahead.* Nat Cell Biol, 2013. **15**(4): p. 338-44.
8. Brabletz, T., *EMT and MET in metastasis: where are the cancer stem cells?* Cancer Cell, 2012. **22**(6): p. 699-701.
9. Kiesslich, T., M. Pichler, and D. Neureiter, *Epigenetic control of epithelial-mesenchymal-transition in human cancer.* Mol Clin Oncol, 2013. **1**(1): p. 3-11.
10. De Craene, B. and G. Berx, *Regulatory networks defining EMT during cancer initiation and progression.* Nat Rev Cancer, 2013. **13**(2): p. 97-110.
11. Javaid, S., et al., *Dynamic chromatin modification sustains epithelial-mesenchymal transition following inducible expression of Snail-1.* Cell Rep, 2013. **5**(6): p. 1679-89.
12. Malouf, G.G., et al., *Architecture of epigenetic reprogramming following Twist1-mediated epithelial-mesenchymal transition.* Genome Biol, 2013. **14**(12): p. R144.
13. Lombaerts, M., et al., *E-cadherin transcriptional downregulation by promoter methylation but not mutation is related to epithelial-to-mesenchymal transition in breast cancer cell lines.* Br J Cancer, 2006. **94**(5): p. 661-71.
14. Pecot, C.V., et al., *Tumour angiogenesis regulation by the miR-200 family.* Nature Communications, 2013. **4**.
15. Splinter, E., et al., *CTCF mediates long-range chromatin looping and local histone modification in the beta-globin locus.* Genes Dev, 2006. **20**(17): p. 2349-54.
16. Hou, C., R. Dale, and A. Dean, *Cell type specificity of chromatin organization mediated by CTCF and cohesin.* Proc Natl Acad Sci U S A, 2010. **107**(8): p. 3651-6.
17. Rhodes, J.M., M. McEwan, and J.A. Horsfield, *Gene regulation by cohesin in cancer: is the ring an unexpected party to proliferation?* Mol Cancer Res, 2011.

9(12): p. 1587-607.
18. Yun, J., et al., *Reduced cohesin destabilizes high-level gene amplification by disrupting pre-replication complex bindings in human cancers with chromosomal instability.* Nucleic Acids Res, 2015.
19. O'Neil, N.J., D.M. van Pel, and P. Hieter, *Synthetic lethality and cancer: cohesin and PARP at the replication fork.* Trends Genet, 2013. **29**(5): p. 290-7.
20. Losada, A., *Cohesin in cancer: chromosome segregation and beyond.* Nat Rev Cancer, 2014. **14**(6): p. 389-93.
21. Xu, H., et al., *Enhanced RAD21 cohesin expression confers poor prognosis and resistance to chemotherapy in high grade luminal, basal and HER2 breast cancers.* Breast Cancer Res, 2011. **13**(1): p. R9.
22. Yamamoto, G., et al., *Correlation of invasion and metastasis of cancer cells, and expression of the RAD21 gene in oral squamous cell carcinoma.* Virchows Arch, 2006. **448**(4): p. 435-41.
23. Scheel, C. and R.A. Weinberg, *Cancer stem cells and epithelial-mesenchymal transition: concepts and molecular links.* Semin Cancer Biol, 2012. **22**(5-6): p. 396-403.
24. Ku, J.L. and J.G. Park, *Biology of SNU cell lines.* Cancer Res Treat, 2005. **37**(1): p. 1-19.
25. Kang, M.J., et al., *Proteomic analysis reveals that CD147/EMMPRIN confers chemoresistance in cancer stem cell-like cells.* Proteomics, 2013. **13**(10-11): p. 1714-25.
26. Sajithlal, G.B., et al., *Permanently blocked stem cells derived from breast cancer cell lines.* Stem Cells, 2010. **28**(6): p. 1008-18.
27. Song, S.H., C. Hou, and A. Dean, *A positive role for NLI/Ldb1 in long-range beta-globin locus control region function.* Mol Cell, 2007. **28**(5): p. 810-22.
28. Song, S.H., et al., *Multiple functions of Ldb1 required for beta-globin activation during erythroid differentiation.* Blood, 2010. **116**(13): p. 2356-64.
29. Yun, J., et al., *Gene silencing of EREG mediated by DNA methylation and histone modification in human gastric cancers.* Lab Invest, 2012. **92**(7): p. 1033-44.
30. Dekker, J., et al., *Capturing chromosome conformation.* Science, 2002. **295**(5558): p. 1306-11.
31. Tolhuis, B., et al., *Looping and interaction between hypersensitive sites in the active beta-globin locus.* Mol Cell, 2002. **10**(6): p. 1453-65.
32. Spilianakis, C.G., et al., *Interchromosomal associations between alternatively expressed loci.* Nature, 2005. **435**(7042): p. 637-45.
33. Hagege, H., et al., *Quantitative analysis of chromosome conformation capture assays (3C-qPCR).* Nat Protoc, 2007. **2**(7): p. 1722-33.
34. Kim, H.P., et al., *Testican-1-mediated epithelial-mesenchymal transition signaling confers acquired resistance to lapatinib in HER2-positive gastric cancer.* Oncogene, 2014. **33**(25): p. 3334-41.
35. Ocana, O.H., et al., *Metastatic colonization requires the repression of the epithelial-mesenchymal transition inducer Prrx1.* Cancer Cell, 2012. **22**(6): p. 709-24.

36. Bernstein, P.L., et al., *Control of c-myc mRNA half-life in vitro by a protein capable of binding to a coding region stability determinant.* Genes Dev, 1992. **6**(4): p. 642-54.
37. Herrick, D.J. and J. Ross, *The half-life of c-myc mRNA in growing and serum-stimulated cells: influence of the coding and 3' untranslated regions and role of ribosome translocation.* Mol Cell Biol, 1994. **14**(3): p. 2119-28.
38. Lee, J.M., et al., *The epithelial-mesenchymal transition: new insights in signaling, development, and disease.* J Cell Biol, 2006. **172**(7): p. 973-81.
39. Oft, M., et al., *TGF-beta1 and Ha-Ras collaborate in modulating the phenotypic plasticity and invasiveness of epithelial tumor cells.* Genes Dev, 1996. **10**(19): p. 2462-77.
40. Xu, J., S. Lamouille, and R. Derynck, *TGF-beta-induced epithelial to mesenchymal transition.* Cell Res, 2009. **19**(2): p. 156-72.
41. Grande, M., et al., *Transforming growth factor-beta and epidermal growth factor synergistically stimulate epithelial to mesenchymal transition (EMT) through a MEK-dependent mechanism in primary cultured pig thyrocytes.* J Cell Sci, 2002. **115**(Pt 22): p. 4227-36.
42. Mamuya, F.A. and M.K. Duncan, *aV integrins and TGF-beta-induced EMT: a circle of regulation.* J Cell Mol Med, 2012. **16**(3): p. 445-55.
43. Desgrosellier, J.S. and D.A. Cheresh, *Integrins in cancer: biological implications and therapeutic opportunities.* Nat Rev Cancer, 2010. **10**(1): p. 9-22.
44. Maschler, S., et al., *Tumor cell invasiveness correlates with changes in integrin expression and localization.* Oncogene, 2005. **24**(12): p. 2032-41.
45. Fang, Z., et al., *Functional elucidation and methylation-mediated downregulation of ITGA5 gene in breast cancer cell line MDA-MB-468.* J Cell Biochem, 2010. **110**(5): p. 1130-41.
46. Shipitsin, M., et al., *Molecular definition of breast tumor heterogeneity.* Cancer Cell, 2007. **11**(3): p. 259-73.
47. Mani, S.A., et al., *The epithelial-mesenchymal transition generates cells with properties of stem cells.* Cell, 2008. **133**(4): p. 704-15.
48. Steeg, P.S., *Tumor metastasis: mechanistic insights and clinical challenges.* Nat Med, 2006. **12**(8): p. 895-904.
49. Nesti, L.J., et al., *TGF-beta1 calcium signaling increases alpha5 integrin expression in osteoblasts.* J Orthop Res, 2002. **20**(5): p. 1042-9.
50. Munger, J.S., et al., *The integrin alpha v beta 6 binds and activates latent TGF beta 1: a mechanism for regulating pulmonary inflammation and fibrosis.* Cell, 1999. **96**(3): p. 319-28.
51. Aluwihare, P., et al., *Mice that lack activity of alphavbeta6- and alphavbeta8-integrins reproduce the abnormalities of Tgfb1- and Tgfb3-null mice.* J Cell Sci, 2009. **122**(Pt 2): p. 227-32.
52. Annes, J.P., et al., *Integrin alphaVbeta6-mediated activation of latent TGF-beta requires the latent TGF-beta binding protein-1.* J Cell Biol, 2004. **165**(5): p. 723-34.
53. Margadant, C. and A. Sonnenberg, *Integrin-TGF-beta crosstalk in fibrosis, cancer*

and wound healing. EMBO Rep, 2010. **11**(2): p. 97-105.
54. Munger, J.S. and D. Sheppard, *Cross talk among TGF-beta signaling pathways, integrins, and the extracellular matrix.* Cold Spring Harb Perspect Biol, 2011. **3**(11): p. a005017.
55. Ohkubo, T. and M. Ozawa, *The transcription factor Snail downregulates the tight junction components independently of E-cadherin downregulation.* J Cell Sci, 2004. **117**(Pt 9): p. 1675-85.
56. Yang, J., et al., *Twist, a master regulator of morphogenesis, plays an essential role in tumor metastasis.* Cell, 2004. **117**(7): p. 927-39.
57. Seitan, V.C., et al., *Cohesin-based chromatin interactions enable regulated gene expression within preexisting architectural compartments.* Genome Res, 2013. **23**(12): p. 2066-77.
58. van 't Veer, L.J., et al., *Gene expression profiling predicts clinical outcome of breast cancer.* Nature, 2002. **415**(6871): p. 530-6.
59. Atienza, J.M., et al., *Suppression of RAD21 gene expression decreases cell growth and enhances cytotoxicity of etoposide and bleomycin in human breast cancer cells.* Mol Cancer Ther, 2005. **4**(3): p. 361-8.
60. Porkka, K.P., et al., *RAD21 and KIAA0196 at 8q24 are amplified and overexpressed in prostate cancer.* Genes Chromosomes Cancer, 2004. **39**(1): p. 1-10.
61. Massague, J., *TGFbeta in Cancer.* Cell, 2008. **134**(2): p. 215-30.
62. Derynck, R., R.J. Akhurst, and A. Balmain, *TGF-beta signaling in tumor suppression and cancer progression.* Nat Genet, 2001. **29**(2): p. 117-29.
63. Scheel, C., et al., *Paracrine and autocrine signals induce and maintain mesenchymal and stem cell states in the breast.* Cell, 2011. **145**(6): p. 926-40.
64. Visvader, J.E. and G.J. Lindeman, *Cancer stem cells: current status and evolving complexities.* Cell Stem Cell, 2012. **10**(6): p. 717-28.
65. Guler, G., et al., *Stem cell-related markers in primary breast cancers and associated metastatic lesions.* Mod Pathol, 2012. **25**(7): p. 949-55.
66. Zeisberg, M., A.A. Shah, and R. Kalluri, *Bone morphogenic protein-7 induces mesenchymal to epithelial transition in adult renal fibroblasts and facilitates regeneration of injured kidney.* J Biol Chem, 2005. **280**(9): p. 8094-100.
67. Bhola, N.E., et al., *TGF-beta inhibition enhances chemotherapy action against triple-negative breast cancer.* J Clin Invest, 2013. **123**(3): p. 1348-58.
68. Tani, N., et al., *Expression level of integrin alpha 5 on tumour cells affects the rate of metastasis to the kidney.* Br J Cancer, 2003. **88**(2): p. 327-33.
69. Carmona, F.J., et al., *A comprehensive DNA methylation profile of epithelial-to-mesenchymal transition.* Cancer Res, 2014. **74**(19): p. 5608-19.
70. Handoko, L., et al., *CTCF-mediated functional chromatin interactome in pluripotent cells.* Nat Genet, 2011. **43**(7): p. 630-8.
71. Shen, Y., et al., *A map of the cis-regulatory sequences in the mouse genome.* Nature, 2012. **488**(7409): p. 116-20.
72. Chaffer, C.L., et al., *Normal and neoplastic nonstem cells can spontaneously convert to a stem-like state.* Proc Natl Acad Sci U S A, 2011. **108**(19): p. 7950-5.

국문초록

고차원의 크로마틴 구조는 hematopoiesis, erythropoiesis, development 동안 중요한 역할을 한다고 알려 져 있음. 크로마틴 구조 단백질인 cohesin complex는 유전자의 organization을 조절하여 암세포에서의 transcript splicing, 유전자 전사, 크로모좀의 안정성 등을 조절한다고 알려 져 있음. Cohesin complex가 암 발생 과정에 관여한다는 수많은 보고들이 있지만, 이러한 cohesin complex를 매개로하는 크로마틴의 구조조절이 암 발생에 어떠한 매카니즘으로 어떤 영향을 주는지는 자세히 알려 져 있지 않은 상태임.

본 논문에서는 1) 다양한 암에서 보여 지는 amplified copy number를 갖는 유전자들이 cohesin을 매개로 하는 특이적인 long-range chromatin interaction을 유지하고 있음을 밝혔음. Cohesin complex 감소는 MCM7, DNA Pol α, CDC45와 같은 pre-replication complex가 증폭된 유전자의 DNA replication origin으로 유도되는 것을 감소시켰고, 따라서 DNA replication initiation의 저해를 일으켰음을 확인. 이것은 amplified gene의 유전자 수를 감소시키는 결과를 확인. 정리 해 보면, 본 연구를 통해 cohesin complex를 매개로하는 크로마틴의 3차원적 구조가 불안정한 크로모좀을 갖는 다양한 암에서 보이는 gene amplification을 안정화 시키는데 중요한 역할을 함을 확인 함.

다음으로, 본 논문에서는 2) Cohesin complex에 의한 크로마틴 organization이 mesenchymal 유전자들의 발현을 증가시키고 그에 따라 EMT를 일으킴을 확인함. Cohesin complex의 subunit 중 하나인 RAD21을 epithelial 암세포에 knockdown 시켰을 때, EMT 관련 유전자인 TGFB1과 ITGA5 발현이 급격히 증가하였고, 이것들은 direct하게 EMT를 일으켰음을 확인하였음. 각 TGFB1과 ITGA5 유전자상에 결합하는 RAD21을 감소시켰을 때, 각 유전자에서 특이적으로 일어나는 intrachromosomal interaction이 감소 되었고, 이를 통해 active한 유전자 전사적 환경이 유도되어 졌음을 확인. Mesenchymal 특징을 갖는 stem-like cancer cell에서도 이상의 결과와 비슷하게 TGFB1과 ITGA5 두 유전자에서 open chromatin structure를 유지하고 있었으며, 이것은 각 유전자의 높은 발현 레벨과 mesenchymal characteristic과 일치함을 확인. 이 결과들을 종합해 보면, 본 연구를 통해 cohesin을 매개로하는 다이나믹한 3차원적 크로마틴 구조가 cancer에서 보이는 reversible한 metastasis를 조절하는데 있어서 중요한 역할을 함을 알 수 있음.

이상의 두 연구를 통해, chromatin architecture molecule인 cohesin complex를 매개로하는 크로마틴의 3차원적 구조가 여러 가지 메커니즘을 통해 cancer development에 있어서 중요한 역할을 함을 확인하였고, 본 연구를 통한 메커니즘을 이용하여 암을 극복할 수 있는 새로운 치료

전략 및 방법을 제시할 수 있었음.

주 요 어: 암, 크로마틴 다이나믹스, cohesin, 암전이, 항암제내성

학 번: 2009-24114